BRNO UNIVERSITY OF TECHNOLOGY
VYSOKÉ UČENÍ TECHNICKÉ V BRNĚ

CENTRAL EUROPEAN INSTITUTE OF TECHNOLOGY BUT
STŘEDOEVROPSKÝ TECHNOLOGICKÝ INSTITUT VUT

CELLULAR POLYMER NANOCOMPOSITES
CELULÁRNÍ POLYMERNÍ NANOKOMPOZITY

THESIS
TEZE K DIZERTAČNÍ PRÁCI

AUTHOR   Ing. KLÁRA ZÁRYBNICKÁ
AUTOR PRÁCE

SUPERVISOR   prof. RNDr. JOSEF JANČÁŘ, CSc.
VEDOUCÍ PRÁCE

CO-SUPERVISORS   Ing. FRANTIŠEK ONDREÁŠ, Ph.D.
ŠKOLITELÉ SPECIALISTI   Ing. PETR LEPCIO, Ph.D.

BRNO 2021

ABSTRACT

This dissertation thesis deals with the preparation and characterization of polymer nanocomposite foams with a focus on means to control their structure at multiple length scales and application in 3D printing in their fabrication. The aim of this work is to investigate polymer nanocomposite with hierarchical structure – from the nano-, through the micro to macro scale. The structural properties of polymer nanocomposites prepared from glassy polymers by the solvent-casting method were investigated in the first part of the work. It has been shown that the difference in the solubility parameters of the polymer and the solvent plays a crucial role. This finding has been verified for systems containing various nanoparticles, polymers, and solvents. With the knowledge of the general principles controlling the structure of nanocomposites, impact polystyrene filled with nanosilica was investigated in greater detail. These nanocomposites were used for the preparation of nanocomposite foams. The porous structure was achieved using a thermal chemical blowing agent azodicarbonamide. The filaments were extruded and the material was processed by 3D printing into the required shapes and foamed. The result was a hierarchical system with the organization of the structure from nano (organization of nanoparticles), through micro (two-component polymer blend structure and foam structure) to macro scale (foam structure and 3D printed design). The effect of nanoparticles on the structure and the thermal and mechanical properties of polymeric foams were observed. The nanoparticles operate as a nucleating agent in the formation of the foam. Pores are easily formed on their surface so that with the content of nanoparticles in the system smaller pores have been formed, which helped to make the foam fine and homogeneous. The presence of nanoparticles changed the surface energy of the blowing agent grains, thanks to which it decomposed at lower temperatures and foaming was even faster. At the same time, nanoparticles have the potential to reinforce foam walls and thus improve mechanical properties. 3D printing is a popular and widespread technique, due to its simplicity it is in many laboratories and test institutions, therefore the demand for filaments with special properties is growing. The material developed in this dissertation is essentially a finished and characterized product that could contribute to the satisfaction of this claim.

KEYWORDS

Polymer nanocomposites, foams, nanoparticle organization, cellular composites, hierarchical systems, 3D printing, structure, mechanical properties, HIPS, azodicarbonamide, nanosilica.

ABSTRAKT

Tato dizertační práce se zabývá přípravou a charakterizací nanokompozitních polymerních pěn se zaměřením na strukturu materiálu a aplikaci v 3D tisku. Cílem práce je studium materiálu s vysoce organizovanou hierarchickou strukturou – od nanoměřítka, přes mikroskopickou strukturu po makroskopická tělesa. V první části práce byly řešeny strukturní vlastnosti nanokompozitů připravených z polymerních skel roztokovou metodou. Byl hledán obecně platný trend, pomocí kterého by bylo možné předpovídat disperzi nanočástic v kompozitu. Ukázalo se, že řídícím faktorem může být závislost na rozdílu parametrů rozpustnosti polymeru a rozpouštědla. Tento poznatek byl ověřen na systémech obsahujících různé nanočástice, polymery a rozpouštědla. Se znalostí principů pro řízení struktury nanokompozitů byly připraveny nanokompozity impaktního polystyrenu plněného nanosilikou. Tyto nanokompozity posloužily jako základ pro přípravu polymerních nakompozitních pěn. Porézní struktury bylo dosaženo pomocí termálního chemického nadouvadla azodikarbonamidu. Z těchto materiálů byly extrudovány filamenty, které byly následně zpracovány pomocí 3D tisku do požadovaných tvarů a vypěněny. Výsledkem byla hierarchická struktura s organizací struktury od nano (organizace nanočástic), přes mikro (struktura dvoukomponentní polymerní směsi a struktura pěny) po makroměřítko (struktura pěny a design 3D tisku). Byl pozorován vliv nanočástic na strukturu a termální a mechanické vlastnosti polymerních pěn. Nanočástice fungují při tvorbě pěny jako nukleační činidlo, na jejich povrchu snadno dochází k tvorbě pórů, takže s obsahem nanočástic v materiálu bylo vytvořeno více menších pórů, což napomohlo k homogenitě pěnové struktury. Přítomnost nanočástic změnila povrchovou energii zrn nadouvadla, díky čemuž docházelo k jeho rozkladu za nižších teplot a pěnění bylo i rychlejší. Nanočástice mají zároveň potenciál vyztužit stěny pěny a zlepšit tak mechanické vlastnosti. 3D tisk je oblíbená a hojně rozšířená technika, díky své jednoduchosti je v mnoha laboratořích a zkušebnách, proto roste poptávka po filamentech se speciálními vlastnostmi. Materiál vyvinutý v této dizertační práci je v podstatě hotovým a charakterizovaným produktem, který by mohl přispět k uspokojení této pohledávky.

KLÍČOVÁ SLOVA

Polymerní nanokompozity, pěny, organizace nanočástic, celulární kompozity, hierarchické systémy, 3D tisk, struktura, mechanické vlastnosti, HIPS, azodikarboamid, nanosilika.

TABLE OF CONTENTS

1 INTRODUCTION TO POLYMER NANOCOMPOSITE FOAMS

Future materials and fabrication technologies will need to integrate unprecedented combinations of stiffness, strength, and toughness at low density and environmental friendliness with end-use specific functions, such as super-hydrophobicity, self-cleaning, mechanical and chemical sensing, shape memory, etc. Even the most advanced synthetic composites do not exhibit the desired structural and functional hierarchy that is found in nature´s load-bearing structures. Structures of natural materials are created by self-assembling processes from relatively simple components. For example, nacre is made of stiff but fragile aragonite and tough but weak protein. These components are organized in a precisely defined hierarchical structure (*bricks and mortar*) from nano to macro-scale which can make the final material of nacre stiff and tough simultaneously. [1] Nature materials with a cellular structure are widespread and include wood, cork, plant parenchyma, glass sponge, and even certain bones, such as a vertebra, femoral head, or skull are filled with a spongy structure called trabecular bone. Exceptional mechanical properties of these materials are believed to be due to a functional adaptation of the structure at levels of hierarchy. For example, the honeycomb-like microstructure of wood gives it a high-performance index for resisting bending and buckling. The radial and longitudinal density gradients and fiber-reinforced composite structure make bamboo strong and stiff with significantly low density. The mineralized cylindrical cage skeleton of a deep-sea glass sponge is structured over at least six levels of hierarchy – biogenic silica reduces its stiffness but an architecture provides substantial toughening that overcomes that of technical glass thanks to structuring at the nanometer and at the micrometer level. [2; 3; 4; 5]

Understanding the role of preparation protocol in the morphogenesis of hierarchical nanocomposites is vitally important for the future applications of polymer nanocomposites in high value-added engineering components. The key obstacle in transforming polymer nanocomposites into industrially viable materials lies in our current inability to directly control the nanoparticle organization over multiple length scales on reasonably short production time and with an industrially viable throughput. Numerous polymer nanocomposites have achieved complex structural hierarchy, from the nanometer to micrometer length scales. However, all of these examples are limited in their ability to organize into larger structures, lacking the necessary combination of simple fabrication and mechanical robustness that span length scales greater than tens of microns.

One possible way how to improve the organization to a higher hierarchical level is to use block copolymers (Figure 1). Block copolymer consists of at least two different monomer blocks that can organize into distinct domains consisting of the constituting homopolymers. For example, two-component polymer blend high impact polystyrene (HIPS) consists of microscale polybutadiene rubber (PBR) particles dispersed in a homopolymer polystyrene (PS) matrix. Adding nanoparticles in such a system will result in their different distribution in the different domains enabling a new level of structural organization. [6; 7]
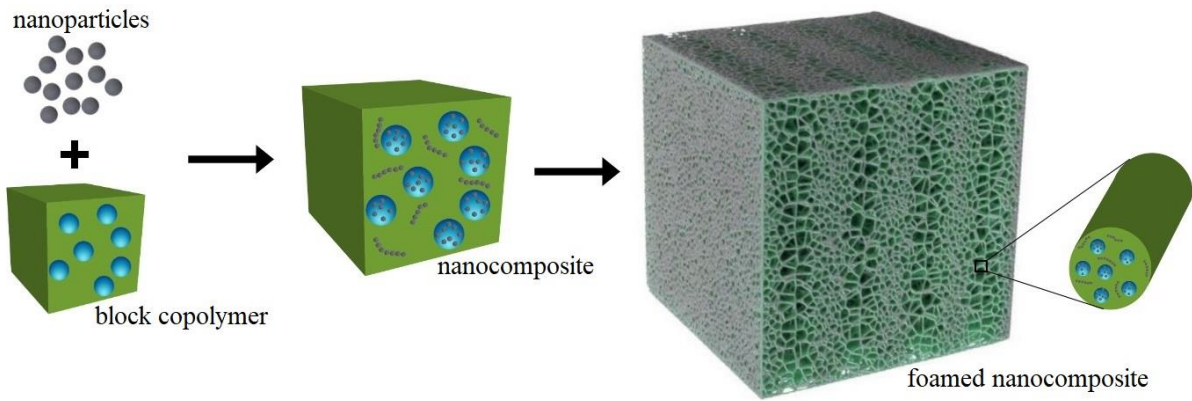
Figure 1: Scheme of foam material with multiple hierarchical levels of structural organization. The state of nanoparticle (grey) dispersion in a polymer matrix (green) represents an organization of material on a nano-scale level. An arrangement of domains (blue) in a block copolymer (e.g., rubber particles in the PS matrix) exhibits the organization of structure on a micro-scale. A micro-to-macro-scale organization is determined by a structure of walls and cells forming polymer foam. The final macroscopic shape of a product could be organized via 3D printing.

Polymer foams are used in many applications because of their excellent thermal and sound insulation properties or because of the flexibility of generating desired morphologies to meet specific applications. On the other hand, foam applications are in many ways limited because of their inferior mechanical strength, poor surface quality and low resistance to high temperatures, and poor dimensional stability. Recently, polymer nanocomposite foams have received increasing attention in both scientific and industrial communities. The combination of functional nanoparticles and foaming technology has a high potential to generate a new class of materials that are lightweight, high strength, and multifunctional. Nano-scaled particles are suitable for microscaled reinforcement (reinforcing of walls of bubble cells), thus achieving the macroscopic mechanical enhancement of foam. Moreover, a small amount of well-dispersed nanoparticles in the polymer may serve as nucleation centers for forming bubbles during the foaming process. Pore nucleation is facilitated and a more homogenous and fine structure of the foam is produced. [8; 9; 10] It has already been shown that nanoparticles can significantly enhance the strength and stiffness of polymer foams and introduce additional functions such as electrical conductivity (with carbon or semiconductive nanoparticles), fire resistance (magnesium hydroxide), hydrophobicity, etc. [11; 12; 13]

Recently, a breakthrough in the 3D printing of versatile, compressible solids with programmable microstructure, customizable shapes, and a tunable mechanical response has been reported. [14; 15] However, the success of 3D printed materials possessing regular cellular architecture as viable replacements for traditional stochastic foams [16; 17; 18] critically depends on their mechanical performance and stability of their micro-architecture under long-term mechanical stress and temperature oscillations. By using polymer nanocomposites instead of neat polymers in this process, it could be envisioned to rapidly fabricate hierarchical, lightweight, functional engineering components possessing the desired balance of stiffness, strength, and toughness.

2 AIMS OF THESIS

1. Finding thermodynamic variables governing nanoparticle spatial organization in polymer solutions.
2. Preparing two-component polymer blend nanocomposites with engineered dispersion of nanoparticles.
3. Optimizing preparation protocol for two-component polymer blend copolymer nanocomposite foams using chemical foaming agents employing 3D printing technology.
4. Analyzing structural-mechanical property relationships in cellular nanocomposites and identifying the role of individual structural variables in these relationships.

3 MATERIALS, PREPARATION PROTOCOL, AND METHODS

3.1 Materials

Polymer matrices

Homopolymeric amorphous polymer glasses were used for the preparation of polymer nanocomposites to establish a principle of governing dispersion state of nanoparticles in matrice via the solvent-casting method, specifically PS (Sigma Aldrich), PC (Makrolon 2407 C, Bayer AG), PMMA (Plexiglass P8N, Evonik) and PVAc (Sigma Aldrich). Commercial grade HIPS PS HI 336M (Synthos Kralupy, Czech Republic) was used. It is a thermoplastic material designed for injection molding with very easy flow and good processability and also very suitable for 3D printing.

Nanoparticles

Two types of nanosilica were used – spherical silica pre-dispersed as a colloidal solution in 30.6 wt. % solution in isopropanol (IPA-ST) or 30.1 wt. % solution in MEK (MEK-ST). Both types of colloidal silica had the same particle diameter (20 nm) and were purchased from Nissan Chemicals. The second type of nanoparticles was powdered fumed silica (Sigma Aldrich) formed by 7 nm particles sintered together into larger aggregates (about 70 nm) as a result of production protocol.

Foaming agent – azodicarbonamide

Azodicarbonamide (1,1′-azobisformamide) is a foaming agent frequently used in the production of thermoplastic. When azodicarbonamide is heated to 165–195 °C an exothermic decomposition occurs. During decomposition at 190 °C is produced 32 wt. % of gasses, 41 wt. % of solid residue and 27 wt. % of sublimate. [19]

Solvents

All solvents used during the preparation of nanocomposites via the solvent-casting method were analytical purity quality (p.a. quality).

3.2 Preparation protocol

3.2.1 Solvent-casting

The appropriate solvent was poured into a glass flask, heated under reflux to 50 °C, and stirred with a magnetic stirrer. When the solvent was heated, the polymer beads were added in the ratio of 150 cm^3 of solvent to 10 g of polymer (corresponds to 6.0 vol. % for solution of PS, 5.2 vol. % for PC, and 5.3 vol. % for PMMA and PVAc), which is in the semi-diluted region of a polymer solution. After the complete dissolving of polymer beads, nanoparticles were added. The mixtures were first ultrasonicated with an ultrasonic homogenizer with titanium tip (Sonopuls, Bandelin) to break aggregates formed during particle storage. Spherical colloidal silica was dispersed in its storage solvent (IPA or MEK) and powdered fumed silica was dispersed in a small amount of solvent used for nanocomposite preparation.

After 60 minutes of stirring solvent-polymer-nanoparticle system, the solution was poured onto a preheated aluminum sheet in an atmospheric drier with a forced airflow to ensure

the most rapid evaporation of the majority solvent and fixing the obtained nanocomposite structure with no additional nanoparticle aggregation caused by sedimentation. The nanocomposite was dried in the atmospheric dryer for 24 hours. The temperature of evaporation was always above the boiling point of the appropriate solvent and above the glass temperature of an appropriate polymer matrix. After drying in the atmospheric drier, the nanocomposite was minced and dried again in a vacuum drier for 6 days to remove residual solvent. The absence of residual solvent and particle loading was checked by TGA.

3.2.2 Foams preparation

The preparation protocol of polymer nanocomposite foams is schematically described in Figure 2. Masterbatch of foaming agent (33.3 wt. %), i.e. polymer granules with concentrated azodicarbonamide, were prepared first. Masterbatch was prepared in laboratory mixer (Plastograph EC plus W 50 EHT, Brabender), where HIPS was heated to 130 °C (actual melt temperature due to shear friction was 150 °C), this temperature was sufficiently high to melt and process HIPS and also sufficiently low that no thermal decomposition of the foaming agent occurred. After melting of HIPS, foaming agent Unicell D200A was added and the compound was blended for 5 minutes with 60 rpm. After colling down, the masterbatch was minced into granules.

Due to the considerable requirement on the fumed nanosilica melt homogenization, the HIPS with fumed nanosilica was not processed in the form of a concentrated masterbatch but was directly pre-mixed at the final concentration of nanoparticles intended for sample preparation in Brabender mixer. To compare nanocomposite structures achieved by different processing methods, the colloidal spherical silica (MEK-ST) was also incorporated into samples by the solvent-casting method described above. Nanocomposites with silica (melt-blended fumed or solvent-casted spherical) were also minced.
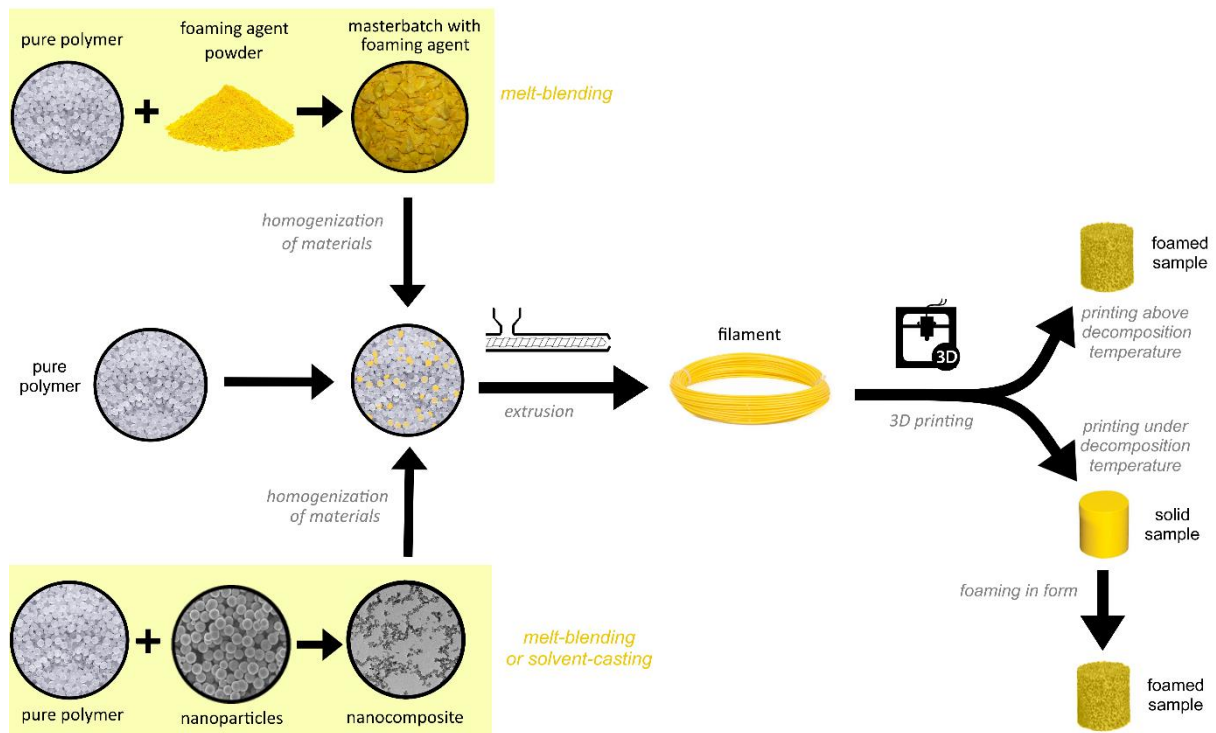
Figure 2: Polymer nanocomposite foam preparation scheme.

Pure HIPS granules (for preparation of pure foams without nanoparticles) or pre-mixed nanocomposite (for preparation of nanocomposite foams) were mixed with the appropriate amount of foaming agent masterbatch in a single-screw extruder (HAAKE PolyLab OS system with HAAKE Rheomex OS, Thermo Scientific) at 180 °C (actual melt temperature 170 °C).

3D printing of test bodies was performed with Reach 3D Printer or Rebel 3D Printer using slicer software Repetier-Host. Bed temperature was set to 75 °C, the diameter of the nozzle was 0.4 mm. Two different nozzle temperatures were chosen, namely 180 °C for printing below the decomposition temperature of the chemical blowing agent and 220 °C for printing above the decomposition temperature of the foaming agent. Quality of the printing, i.e. height of one printed layer varied according to temperature conditions – 0.1 mm layer for printing at 180 °C to reach high quality printed body and 0.3 mm layer for printing at 220 °C to not overpress bubbles formed by the decomposition of blowing agent at the higher temperature.

If the sample was printed under the decomposition temperature of the foaming agent, the entire processing was carefully thermally balanced to allow the polymer to process well, but the blowing agent did not foam. For example, during 3D printing, the temperature processing range was very narrow. At 170 °C, the melt had too high viscosity, did not pass through the nozzle and 3D printing was not possible. Thermal decomposition of the foaming agent occurred at 190 °C, causing undesirable foaming during processing. The products printed under the decomposition temperature of the foaming agent were tested directly after 3D printing or finally foamed at 200 °C in an atmospheric oven (post-processing foaming). Time of post-processing foaming varied according to nanosilica presence – 30 min for samples without nanoparticles, 10 min for samples with 1 wt. % of fumed nanosilica and 5 min for 1 wt. % of spherical nanosilica. The foaming process (Figure 3A) was carried out in a form, its circumference was made of aluminum and the bases were made of glass. The form diameter d_f

was 120 % compared to the diameter of the printed sample d_s. The form height was the same as that of the printed sample $h_f = h_s$. The entire form was carefully heated before sample placement to allow more efficient heat transfer to the bulk of the sample. After foaming, the sample was cooled down to room temperature to fix the formed porous structure.
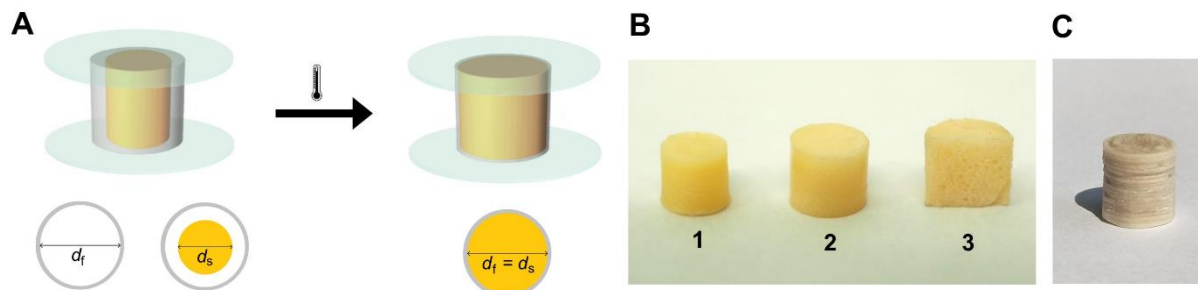
Figure 3: A – Post-processing foaming scheme. **B** – Photo of HIPS samples with 2 wt. % of Unicell D200A. Unfoamed cylinder after 3D printing at 180 °C (1), cylinder foamed to 120 % of diameter at 200 °C for 30 minutes (2) and the foamed cylinder cut in half (3). **C** – Photo of HIPS sample with 2 wt. % of Unicell D200A after 3D printing at 220 °C.

3.3 Methods

Samples for scanning electron microscopy (SEM) or transmission mode (STEM) and confocal laser scanning microscopy (CLSM) observation were broken in liquid nitrogen first. Surface of SEM samples was coated with 10 nm layer of Au deposited by sputtering to ensure better surface conductivity (Coater Leica EM ACE 600). STEM samples for nanoparticle dispersion determination were cut to 50 nm ultramicrotome slices. SEM and STEM samples were observed by the high-resolution microscope Verios 460L (FEI). CLSM samples for pore structure observation were observed on Olympus Lext OLS 4000.

Approximate determination of the thermal stability of the polymer matrix, verification of residual solvent, filler loading, and blowing agent decomposition TGA measurements were done on TGA Discovery (TA Instruments). Temperature ramp 10 °C·min^{-1} to 650 °C in nitrogen atmosphere.

Zeta potential (ζ-potential) of colloidal spherical nanosilica was measured in 1 wt. % concentration in a series of solvents at Zetasizer instrument (Malvern Panalytical).

Tensile tests of filaments and compression tests of 3D printed cylinders were performed on Zwick Roell Z10 device at room temperature. 5 specimens were measured for each sample batch. Filament specimens had a round shape with a gauge length of 100 mm and were tested with strain rate 2 mm·min^{-1}. By tensile tests were evaluated tensile modulus (the maximum of the peak of the first derivation from the stress-strain curve), 0.2 % offset yield strength, tensile strength, and elongation. Directly 3D printed specimens had a cylindric shape with a high of 6 mm and a diameter of 6 mm. Specimens treated by post-processing foaming after 3D printing had a cylindric shape with a high of 6 mm and a diameter of 7.2 mm. Strain rate during compression tests was set to 1 mm·min^{-1}. By compression tests were evaluated compression modulus and 0.2 % offset yield strength. Specific properties were determined by dividing certain property value by the mass density of the material.

4 RESULTS AND DISCUSSION

4.1 Controlling nanocomposite structure

4.1.1 Nanocomposites with homopolymer matrices

This chapter Nanocomposites with homopolymer matrices is based on the published article *Thermodynamic parameters controlling nanoparticle spatial packing in polymer solutions* from authors K. Zarybnicka, F. Ondreas, P. Lepcio, M. Kalina, M. Zboncak, and J. Jancar (*Macromolecules*. 2020, **53**(19), 8704-8713. ISSN 0024-9297. Available at: doi:10.1021/acs.macromol.0c00698). The text is reproduced with permission from [20]. Copyright 2020 American Chemical Society.

4.1.1.1 *General laws controlling morphogenesis in glassy nanocomposites*

The only heteroatom present in the polymers investigated in this thesis (PC, PMMA, and PVAc except for PS with no heteroatom) was oxygen, which interacted with its free electron pairs as a proton acceptor (base). Hence, polymer chains and solvent molecules competed with each other over the acidic silica surface. The polymer-solvent interaction seemed to be one of the dominant parameters in the determination of the nanoparticle organization as will be shown below. Nevertheless, when nanoparticle-solvent interaction was weak, particle-particle and polymer-particle interaction strengths started to play a decisive role in the nanoparticle aggregation process.

The surface chemistry of nanoparticles was recognized as an important parameter influencing the polymer-particle interaction and, consequently, the quality of polymer nanocomposite dispersion. The solubility parameter δ of a particle relates to its surface properties rather than its bulk chemistry. Jouault et al. [21] suggested δ to be one possible criterion for the determination of nanoparticle dispersion in solvent cast polymer nanocomposites. They hypothesized that better solvent for polymer (i.e. difference of solubility parameter between solvent and polymer is very low) reduces dielectric constant $\varepsilon \to$ lowers dissociation of silanol groups (lowers ζ-potential) $\to$ lowers solvation shell and repulsive barrier around particles and contact aggregation may occur.

Nanosilica used in the current experiments contained bare particles with no surface modification. Therefore, the values for bulk silica were used to predict the nanoparticle dispersion state. Lepcio [22; 20] estimated Hansen solubility parameters [23] of silica from the critical concentration of a displacer co-solvent [24] to (18.8 ± 1.0) $(\text{J·cm}^{-3})^{0.5}$, (5.7 ± 0.8) $(\text{J·cm}^{-3})^{0.5}$, and (6.3 ± 0.8) $(\text{J·cm}^{-3})^{0.5}$ for dispersive (energy from dispersion forces between molecules), polar (energy from the dipolar intermolecular force between molecule), and hydrogen bonding (energy from hydrogen bonds between molecules) partial solubility parameter, respectively. Hildebrant solubility parameter of bare silica δ_{silica} (spherical colloidal silica) could be then calculated as:

$$\delta_{\text{silica}} = \sqrt{4 \cdot \delta_{\text{D}} + \delta_{\text{P}} + \delta_{\text{H}}} = 20.6 \text{ MPa}^{0.5}. \tag{1}$$

According to this δ_{silica} value, the affinity of polymers to silica scales in the order PC > PVAc > PMMA > PS as determined by the difference in the solubility parameters of silica and appropriate polymer ($1 < 1.1 < 1.6 < 1.9$ MPa$^{0.5}$).

Following the acid-base competition theory, the polarity of the particles and the polymer must be taken into account. While the polarity of particles was fixed for all samples using the same silica nanoparticles, the polymer dipole moments were evaluated according to the dipole moments of their monomers. Methyl methacrylate monomer (PMMA) has a dipole moment of 1.67 D, vinyl acetate (PVAc) has a dipole moment of 1.79 D, styrene (PS) has a dipole moment of 0.12 D and the average of carbon acid and Bisphenol A (PC) dipole moment is 0.50 D. It has been previously reported [25; 21] that the dispersing solvent can control the nanoparticle spatial organization in polymer nanocomposites. Nevertheless, the current data of this work shows that the type of polymer matrix also had an essential effect on the resulting nanoparticle organization and the relative change in nanocomposite properties induced by nanoparticles. Therefore, all interactions between polymer-solvent-particle should be considered.

For the purpose of quantitative analysis, individually dispersed particles, aggregates, and clusters were considered as basic elements characterizing the actual nanoparticle dispersion. The size of all organization types formed in the structure of nanocomposites (individually dispersed particles, chain bound clusters, and agglomerates) was collectively called the size of the agglomerates d_w. Size of elements d_w was divided by single nanoparticle diameter d_{sp} and related to the polymer-solvent interaction strength evaluated by the reciprocal absolute difference in the Hildebrand solubility parameters δ of solvent and polymer $1/|\delta_{solvent}-\delta_{polymer}|$ as shown in Figure 4.

There are at least two main regimes of nanoparticle organizational states as indicated by the two auxiliary solid lines in Figure 4. The systems with very low reciprocal absolute difference between the Hildebrand solubility parameters of solvent and polymer $1/|\delta_{solvent}-\delta_{polymer}|$ could be possibly attributed to the third independent mechanism as will be discussed later. In this region (bottom left corner in Figure 4), dispersion of individual particles is expected. At around $1/|\delta_{solvent}-\delta_{polymer}|$ of 0.6 MPa$^{-0.5}$, the dependence splits into two independent regimes. Systems on the lower curve keep a relatively good dispersion of individual nanoparticles, very small aggregates of approximately 2–8 nanoparticles or chain bound clusters (i.e. good dispersion in global), while the systems on the upper curve show a large systematic increase of element size with increasing $1/|\delta_{solvent}-\delta_{polymer}|$. A detailed characterization of the different nanoparticle self-assembly regimes will follow.
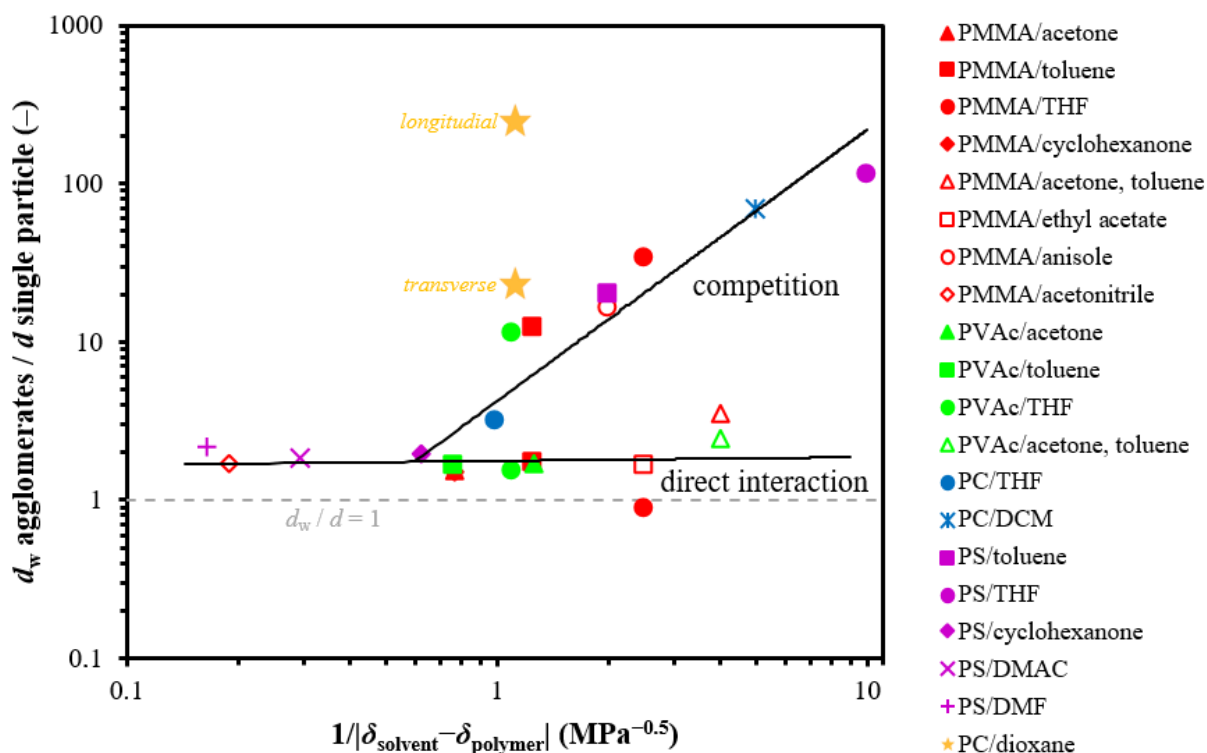
Figure 4: The ratio of agglomerate size d_w to the single-particle diameter d_{sp} for spherical nanosilica nanocomposites depicted as the dependence on the reciprocal absolute difference in the Hildebrand solubility parameters of solvent and polymer. The two populations of dispersed individual particles and aggregated populations in PMMA-THF and PVAc-THF and the two populations of small and larger aggregates in PMMA-toluene composites were plotted separately as two points for each system. The anisotropic microfibrous structure formed in PC-dioxane was a specific case and thus was not included in the trends defined by the solid lines. Raw data are available in the appendix.

It is supposed that the high negative charge on silica manifested by the high negative value of ζ-potential is caused by strong solvation. Therefore, in such systems, solvent-nanoparticle interaction won the competition against the polymer-nanoparticle counterpart for the particle surface and almost no polymer segments could adsorb. The current results are consistent with the previous study [25] which correlated the effective hydrodynamic volume of nanoparticles in a polymer solution and the enthalpy of the acid-base interaction between solvent and particle with the nanoparticle organization. Good dispersion was observed at intermediate solvent-particle interaction strength altogether with little to no traces of polymer adsorption shell as evidenced by the effective hydrodynamic volume. Suggestively, the dispersion stability could be attributed to the combination of the solvation shell and weakly absorbed polymer shell around the particles. This hypothesis is supported by many systems in the bottom left corner of Figure 4. All these systems showed a relatively low ζ-potential of less than –20 mV which corresponds to weak electrorepulsive stability as the threshold of incipient electrorepulsive stability of colloidal solutions is considered about ±10 mV. [26]

Strong particle-solvent interaction would normally provide a strong solvation shell and a good electrorepulsive stability, the solvent would act as a displacer preventing polymer adsorption on the nanoparticle surface. [21] However, in the presence of polymer, it reportedly caused a depletion attraction which could compromise the otherwise good dispersion of nanoparticles [25] as it can be seen on PC-DCM-silica system where large aggregates were found (Figure 4). PC had the strongest interaction strength with the silica surface

13

of the investigated polymers, and yet, the aggregation tendency was imposed by an appropriate solvent. Hence, it is apparent that the polymer-particle interaction could be equaled or even outweighed by the role of solvent and the strong polymer-particle interaction alone is not always a sufficient condition to obtain a good dispersion of nanoparticles. The difference between the solubility properties of the competing polymer and solvent is the key parameter that, together with the particle-particle interaction assessed by ζ-potential, governs the nanocomposite structure. This finding is consistent with the seemingly superior importance of the solvent and the known significance of the polymer matrix.

Moreover, stabilization of good dispersion possibly relies also on the chain conformation rather than the surface interaction strength alone. With a larger difference in solubility parameters between solvent and polymer (or its small reciprocal value), the polymer coil was more packed, the radius of polymer coil $r_{polymer}$ decreased (Figure 5A), as verified by DLS measurement (Figure 5C). Unlike other polymers, PS had an approximately constant coil radius in the investigated range of solvents. It could be possibly caused by its low polarity, relatively high molecular weight, chain rigidity, and polydispersity.

In the solution state, when the compact coil adsorbs on the surface of the silica, a stiffer layer of the modified matrix will be created around the particle and therefore another particle cannot access the first particle. The packed coil in a poor solvent adsorbs to one particle surface and forms a compact polymer shield layer which prevents direct particle-particle contact. Thus, a layer of an adsorbed polymer is formed around the particle, followed by a polymer bulk, thereby stabilizing good dispersion. Similar behaviour was observed by Jouault et al. [21] when they described the adsorption of poly(2-vinyl pyridine) (P2VP) onto nanosilica surface in MEK. The resulting "hairy" particles were sterically stabilized against agglomeration.
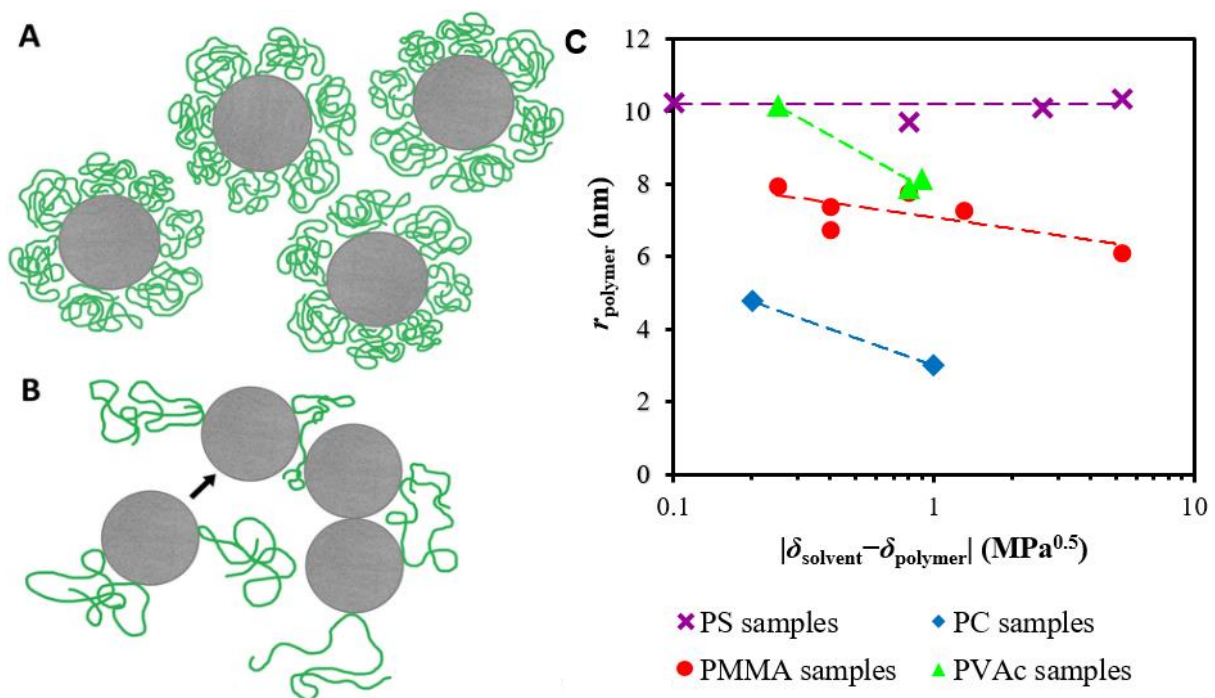
Figure 5: A – Nanoparticles with an adsorbed layer of compact polymer coils formed in a poor solvent. **B** – Nanoparticles with adsorbed flexible expanded polymer coils formed in a good solvent. Graph **C** – Radius of polymer coils in solutions of various solvents (determined by DLS) dependence on the difference of solubility parameter between solvent and polymer. Dashed lines are for eye guidance.

14

On the other hand, expanded coil (Figure 5B) in a good solvent (the small difference in solubility parameter or its large reciprocal value) can more readily act as bridging molecules and thus promote a couple of the particles over short distances and hold the particles together, creating clusters. Furthermore, more flexible expanded coil adsorbed on one particle is not such a difficulty to another particle to approach and create contact aggregation.

Low negative values of ζ-potential above -5 mV and below approximately -10 mV, which is the threshold for incipient electro-repulsive stability [26], allow for both particle-particle agglomeration and acid-base adsorption of polymer onto silica taking place simultaneously. The latter process led to a formation of an adsorbed polymer shell which could stabilize a relatively good dispersion while the former yielded large aggregates. Unlike the previous case, particle-polymer interactions seem to have an important role in this mechanism of nanoparticle assembly.

The stability of silica in toluene was such low (ζ-potential of -3.3 mV) that the polymer adsorption was competed by rapid nanoparticle contact aggregation. While this process was of a completely different nature than the depletion attraction, as was shown in the previous study [25], the formed nanocomposite structures followed in both cases a similar dependence on $1/|\delta_{\text{solvent}}-\delta_{\text{polymer}}|$ (Figure 4), though it is not clear whether this was a coincidence or a systematic behaviour.

Contact aggregates observed in toluene nanocomposites showed less symmetric and more chaotic organization which was possibly attributed to their kinetic origin compared to the thermodynamic one of the aggregates formed due to the depletion attraction. [25] Large aggregates were observed for PS-toluene system, which showed the lowest particle-polymer interaction strength and the greatest $1/|\delta_{\text{solvent}}-\delta_{\text{polymer}}|$ values of all the toluene samples. Two populations of aggregates were found in the PMMA-toluene system suggesting that lessened coil swelling and increased strength of surface interaction helped to prevent nanoparticle aggregation. Finally, polymer adsorption stabilized dispersion of individual nanoparticles and very small clusters/aggregates were formed in PVAc-toluene, where the matrix showed the lowest coil expansion and the strongest nanoparticle-polymer interaction.

Finally, dioxane was a special case since it was the only investigated solvent that acted as an acid towards the silica (ζ-potential of $+0.4$ mV), which means that dioxane and silica should compete together for the basic active sites of the polymer. Moreover, positively charged silica could catalyze the decomposition of dioxane to acetaldehyde and subsequent polymerization of acetaldehyde to oligomeric or polymeric (POE) chains which possibly leads to the exceptionally large nanoparticle assemblies. In silica-PC-dioxane nanocomposite, the 20 nm spherical nanosilica was assembled into 5 μm long microfibres with an aspect ratio of 11 and $d_{\text{w}}/d_{\text{sp}}$ of about 250 and 23.5 for longitudinal and transverse direction, respectively. [27]

The solubility parameters represent the enthalpic parameters in the polymer nanocomposite solutions. It should be taken into account that the dispersion of nanoparticles in a nanocomposite system is also affected by entropic parameters, such as the molecular weight of the polymer matrix. The conclusion of this thesis is based on experimental data, thus the variation of molecular weight across all systems would be beyond the scope. Hashemi et al. [28] observed that the stability of a good dispersion increases with increasing molecular weight.

Due to the larger number of entanglements on the longer chains, the nanoparticles do not have such an opportunity to diffuse freely through the system, and their aggregation is thus to some extent more suppressed. Jouault et al. [21] stated that in the case of really strong adsorption of polymer chains onto nanoparticles surface (e.g. due to strong hydrogen bonds between the silanol groups on the nanoparticle surface and the functional nitrogen groups in P2VP), the good dispersion in polymer nanocomposites is always achieved, independent of matrix molecular weight.

4.1.1.2 Relaxation properties of polymer nanocomposites

The different strengths of the nanoparticle-polymer and the solvent-polymer interaction also affected the thermomechanical properties of the investigated nanocomposites. The T_g of the nanocomposites prepared in the THF was determined employing the DSC ($10\ °C·min^{-1}$) and compared to the glass transition temperature of the neat polymer matrices, $T_{g,\ matrix}$. The change of nanocomposite T_g from the $T_{g,\ matrix}$ was determined as:

$$\Delta T_g = T_g - T_{g,\ matrix}. \tag{2}$$

In agreement with the existing models, the T_g increased with increasing heating rates. Modified Arrhenius equation [29] can then be used for calculation of the activation energy of glass transition, $E_{A,\ Tg}$:

$$\ln q = \ln q_0 - \frac{E_{A,\ Tg}}{R} \cdot \frac{1000}{T_g}, \tag{3}$$

where q is the heating rate ($K·min^{-1}$), q_0 is the preexponential factor with the same unit as the unit of heating rate, R is the universal gas constant ($J·K^{-1}·mol^{-1}$). The $E_{A,\ Tg}$ (kJ) can be calculated from the slope of the linear dependence of the $\ln q$ vs. $1/T_g$ plot. The relative $E_{A,\ Tg}$ was calculated by dividing $E_{A,\ Tg}$ of nanocomposite by activation energy of neat polymer matrix, $E_{A,\ Tg\ matrix}$:

$$\text{rel. } E_{A,\ Tg} = \frac{E_{A,\ Tg}}{E_{A,\ Tg\ matrix}}. \tag{4}$$

Rel. E_A and ΔT_g were related to the absolute difference between the solubility parameters of solvent and polymer $|\delta_{solvent} - \delta_{polymer}|$ (Figure 7A). The increase of $|\delta_{solvent} - \delta_{polymer}|$ directly correlates with the decrease of the size of aggregates d_w as shown in Figure 4 . The function of rel. E_A, and ΔT_g on size of agglomerates d_w (Figure 6) was consistent with this finding. Therefore, further in the text, it is inherently considered that the increase of $|\delta_{solvent} - \delta_{polymer}|$ includes the decrease of d_w.

Although the individual particles in the PVAc-THF and PMMA-THF samples exceeded the aggregate population in frequency, a large number of primary particles with the inaccessible surface area were concentrated in the aggregates reducing the overall available active particle surface. Since this reduction had a significant effect on relaxation behaviour, the d_w values

for PMMA and PVAc were taken from the larger of the two populations present in these systems.
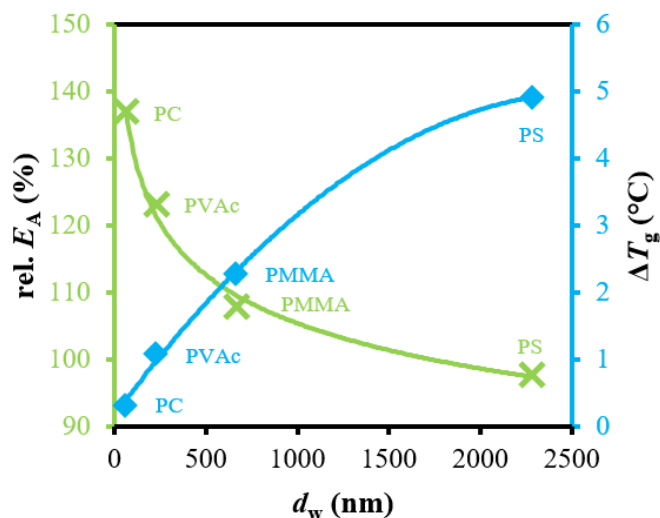
Figure 6: Dependence of the relative glass transition activation energy (E_A) and the increase of glass transition temperature (ΔT_g) on the element size d_w.

A gradual increase in rel. E_A accompanied the increasing $|\delta_{solvent} - \delta_{polymer}|$, i.e., decreasing element size d_w as expected. Polymer chains formed an affected polymer layer with retarded molecular packing and dynamics around the solid surface of particles due to the attractive interactions. [11; 25] The effective interfacial surface increases with increasing $|\delta_{solvent} - \delta_{polymer}|$ (decreasing d_w); therefore, the number of polymer chains with retarded dynamics also increased for smaller particles and so did the energy expenditure required for the release of chain segmental scale movement. However, ΔT_g grew with decreasing $|\delta_{solvent} - \delta_{polymer}|$ (increasing d_w) despite it was expected that ΔT_g should follow the same trend as rel. E_A and increase with increasing the effective interfacial area. [11; 25; 30; 31; 32; 33; 34; 35]

Nevertheless, the previous investigations were performed on a system with constant chemical composition and the interfacial area controlled via nanoparticle concentration. Therefore, the strength of the silica-polymer interactions expressed by the solubility parameters (Figure 7B) was investigated. It was expected that the attraction between the particle surface and the polymer chains was stronger for lower values of the absolute difference $|\delta_{silica} - \delta_{polymer}|$. PC had the strongest attraction to the nanosilica surface while PS had the weakest. Rel. E_A increased with the increasing interaction strength in accordance with expectations; however, ΔT_g followed the opposite trend again.
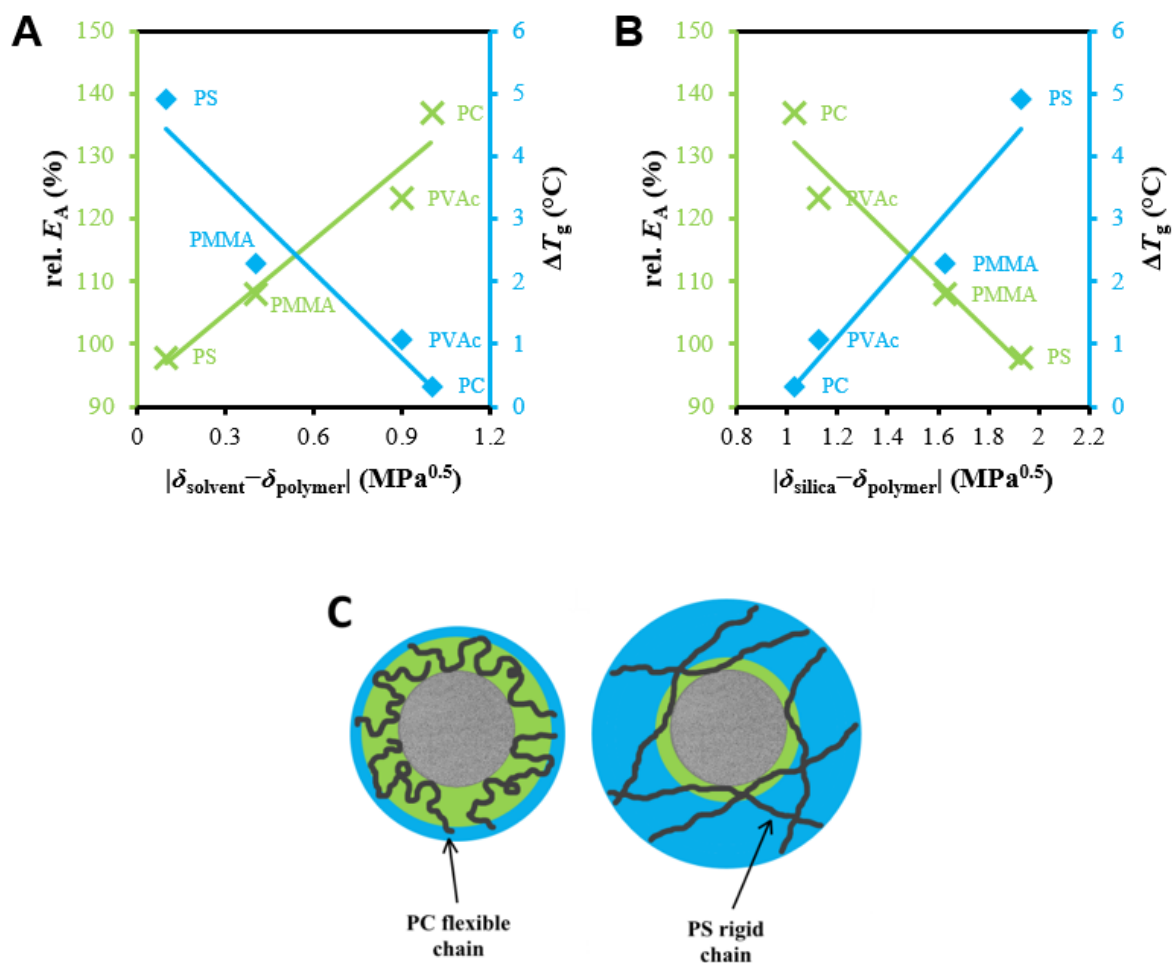
Figure 7: A – Dependence of the relative activation energy of glass transition (E_A) and glass transition temperature (ΔT_g) on the absolute difference in solubility parameters of solvent and polymer and **B** – on the difference in Hildebrand's solubility parameters of silica and polymer. Raw data are available in the appendix. **C** – An illustrative picture shows the difference between the adsorption of flexible PC chains and rigid PS chains onto nanoparticle surface, green color represents the immobilized layer, blue color represents the frustrated layer.

Before further interpretation, it would be useful to recall the detailed physicochemical situation of the affected polymer layer [11; 25; 30] (Figure 7C) and the mechanisms of chain interaction with nanoparticle surface [36; 37; 38; 39; 40]. It is assumed that the affected polymer layer around nanoparticles consists of the immobilized and frustrated polymer layer. The immobilized polymer layer consists of tightly adsorbed polymer segments that directly adheres to the surface of the nanoparticle with greatly retarded chain dynamics and a typical thickness of 1–3 nm [41; 42; 43; 44] while the frustrated layer is formed by chains interacting with the immobilized polymer layer via intramolecular (chain connectivity) or intermolecular (entanglements) interaction. [11; 45] The packing of the frustrated layer is also influenced, and its dynamics retarded, but to a much lesser extent compared to the immobilized layer. On the other hand, the thickness of the frustrated layer is larger   (10–20 nm) [46; 30; 44; 47], thus, it occupies a larger overall volume of the material.

Tannenbaum and Ciprari et al. [36; 37] assumed that polymers with a strong attraction to the particles tend to adsorb with a larger number of their segments, possibly forming trains on the nanoparticle surface. Subsequently, they form short loops and do not affect a large number of surrounding chains due to short effective length and a frustrated layer. Weakly binding

18

polymers prefer the adsorption of only one or a very few segments and form long loops with long effective length forming a large frustrated layer.

Cheng et al. [38] investigated the dependence of the thickness of the interfacial layer between the polymer matrix and the polymer rigidity defined through the characteristic ratio C_∞. They revealed that the thickness of the interfacial layer and length scale of dynamic heterogeneity in polymer nanocomposites increased with increasing polymer C_∞. Jouault et al. [39] determined a greater amount of bound polymer for weakly interacting PS than for attractively interacting PMMA matrix in a series of nanosilica filled nanocomposites.

Generalizing the results of this dissertation work altogether with the other available data, it was assumed that the interaction strength and chain conformation (stiffness) control the size of the affected polymer layer and the thickness ratio between the immobilized and the frustrated layers within it. Moreover, it was suggested that glass transition temperature T_g and activation energy E_A are susceptible to individual layers in different ways. Rel. E_A is assumed to be susceptible mainly by the properties of the immobilized layer formed by adsorbed polymer segments that directly adhere to the nanoparticle surface. The stronger the interaction between polymer and silica was, the thicker the immobilized layer with more retarded dynamics was formed. In turn, more energy was required to release the chain conformations. The rel. E_A scaled in the following order: PC > PVAc > PMMA > PS which agrees well with the proposed hypothesis. ΔT_g is expected to be primarily dependent on the properties of the frustrated layer. [30] Flexible chains (like PC) did not transfer the immobilization retardation over long distances; hence, the frustration layer was rather thin. In contrast, the rigid PS chains transferred the retardation furthest to the bulk polymer more effectively and the frustration layer around the nanoparticles was thicker, shifting the glass transition to the higher temperature. Confirming the hypothesis, chain flexibility, and interaction strength decreased while ΔT_g increased in the following order: PC > PVAc ≥ PMMA > PS. PC had the most flexible chains, which characteristic ratio C_∞ is 2.4, the characteristic ratio of PVAc and PS is 8.9 and 10.2, respectively. PMMA's C_∞ is dependent on the chain tacticity – isotactic PMMA has $C_\infty = 9.2–10.7$, syndiotactic 7.3–8.4 and atactic PMMA is assumed to have the greatest stiffness. [48] The PMMA used in this study was atactic with a high portion of syndiotactic chains. [49] In the light of the presented evidence, the widespread simple expectation that strong polymer-particle interactions yield the best possible enhancement of all thermo-mechanical properties seems no longer valid. More likely, the complex interplay of several mechanisms operating at the nano-scale has to be considered. This complex situation can be easily solved by taking the various thicknesses of immobilized and frustrated layers into account.

4.1.2 Nanocomposites with HIPS matrix

For the preparation of HIPS nanocomposite the cyclohexanone solvent was used (in this solvents, the best dispersion of small silica clusters in the glassy PS phase was achieved.). Cyclohexanone dissolved both, the PS matrix and rubber particles. The cyclohexanone solution was clear when viewed with the naked eye. From DLS histogram, it is evident that the ratio of the intensity representing polymer coils significantly exceeded that of the rubber particles. Thus, most rubber particles were dissolved into individual polymer chains dispersed homogeneously in colloidal solution.
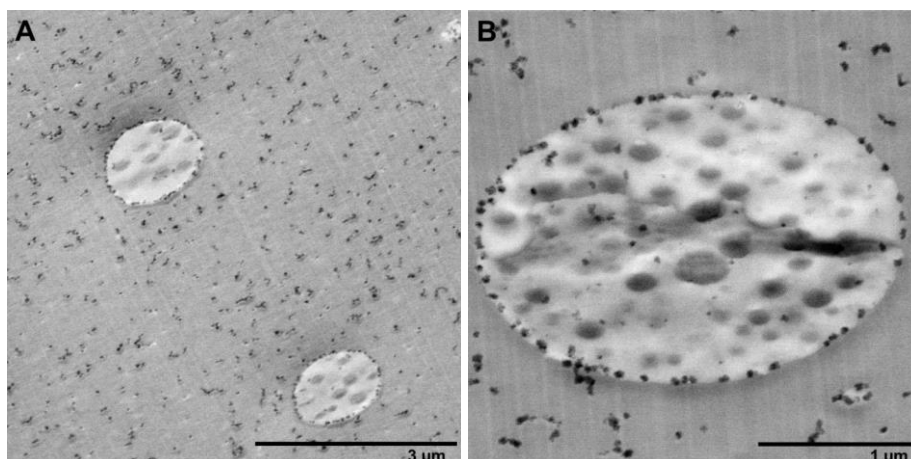
Figure 8: TEM images of HIPS nanocomposite prepared in cyclohexanone with 1 vol. % of spherical silica. **A** – Overview of good dispersion. **B** – Occluded particle detected in BF mode.

To simplify the preparation protocol, many experiments were first performed with fumed silica particles incorporated into the HIPS using melt-blending (**Figure 9**).
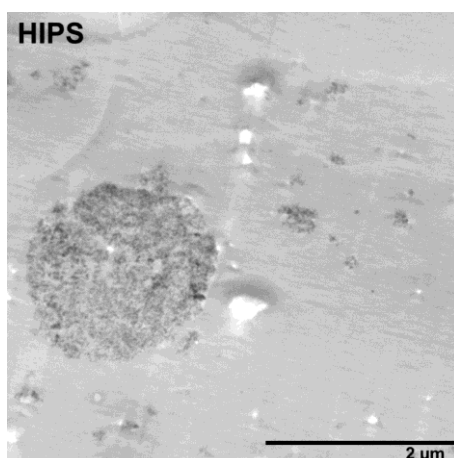
Figure 9: TEM image of nanocomposite with 1 vol. % of fumed silica prepared by the melt-blending method. HIPS sample with the holes caused by the rupture of the rubber particles during ultramicrotome cutting.

4.2 Structural and thermal analysis of foams
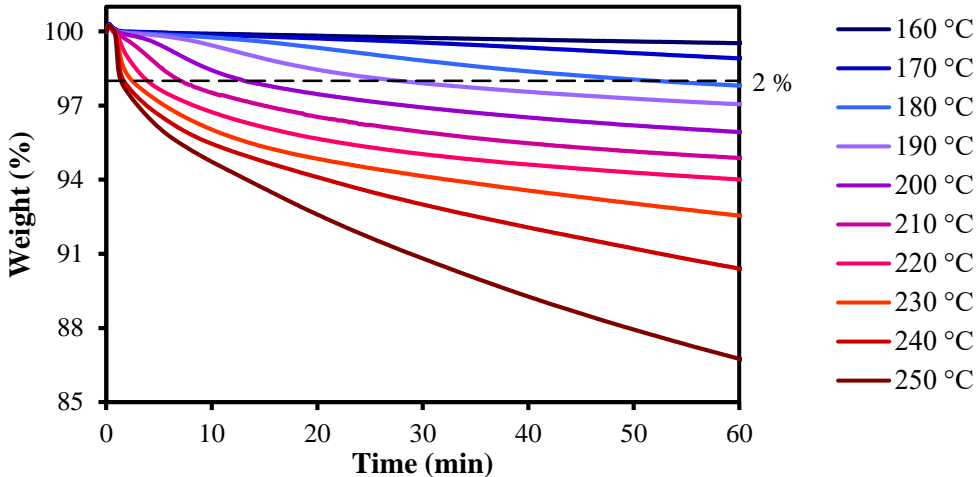
4.2.1 Thermal decomposition of the foaming agent

The optimum foaming temperature and time were determined employing the TGA, in which the foaming process in the air was simulated. One-hour isothermal hold of pure azodicarbonamide or HIPS with 2 wt. % of azodicarbonamide at constant temperature is shown in Figure 10. The temperature range for individual measurements was 160–250 °C in 10 °C steps. It seems clear, that significant decomposition of the pure blowing agent and gas release occurred at temperatures above 200 °C. In the case of HIPS with 2 wt. % of the foaming agent, degradation of the polymer matrix in an oxidative atmosphere at elevated temperatures was observed. The dashed line in the graph represents 2 wt. %, i.e. the limit at which the whole amount of the foaming agent would theoretically decompose while maintaining all the polymer

matrix. As can be seen, when the sample was foaming at higher temperatures, there was a massive degradation of the HIPS matrix, so the high temperature was undesirable.

Pure foaming agent (azodicarbonamide):
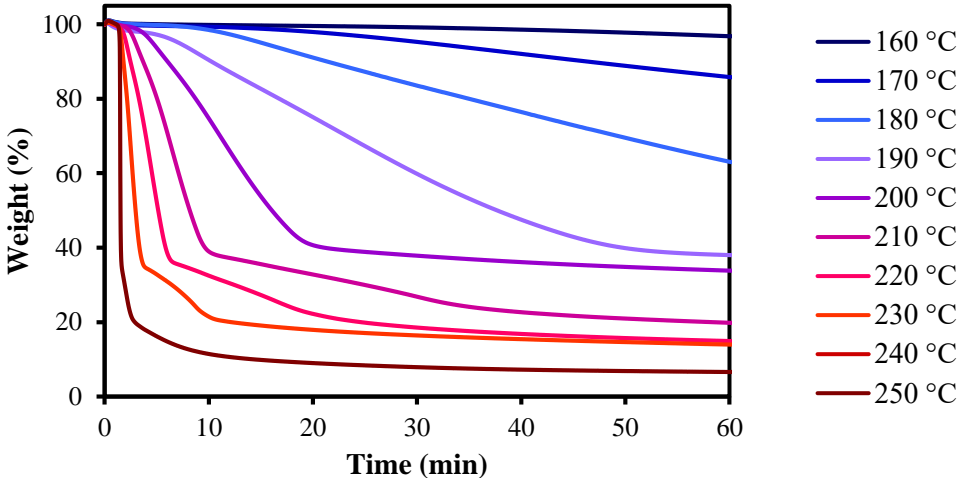
2 wt. % of foaming agent in HIPS:

Figure 10: TGA simulation of foaming process in air atmosphere – isothermal hold of the material at different temperatures for 60 minutes. The upper graph shows the decomposition of the pure foaming agent (azodicarbonamide). The lower graph shows the thermal decomposition of the HIPS sample with 2 wt. % of foaming agent. The dashed line defines the content of the foaming agent in the sample.

When HIPS with the blowing agent was extruded from the 3D printer at 180 °C, almost no blowing agent decomposed, because decomposition of azodicarbonamide at this temperature was very slow, and the stay of the polymer in the heated printer extruder and nozzle was short. At 220 °C, the probability of HIPS degradation was faster, however, the stay of melted polymer in the printer and the heated nozzle was short but the time was sufficient for the blowing agent to decompose and cause foaming.

Hence, foaming at 200 °C for 30 min after 3D printing at 180 °C was, found to provide optimal conditions – azodicarbonamide decomposition was fast enough for a sufficiently long time to produce the desired foam structure while minimizing HIPS degradation. With shorter foaming times, the HIPS degradation was even more suppressed.
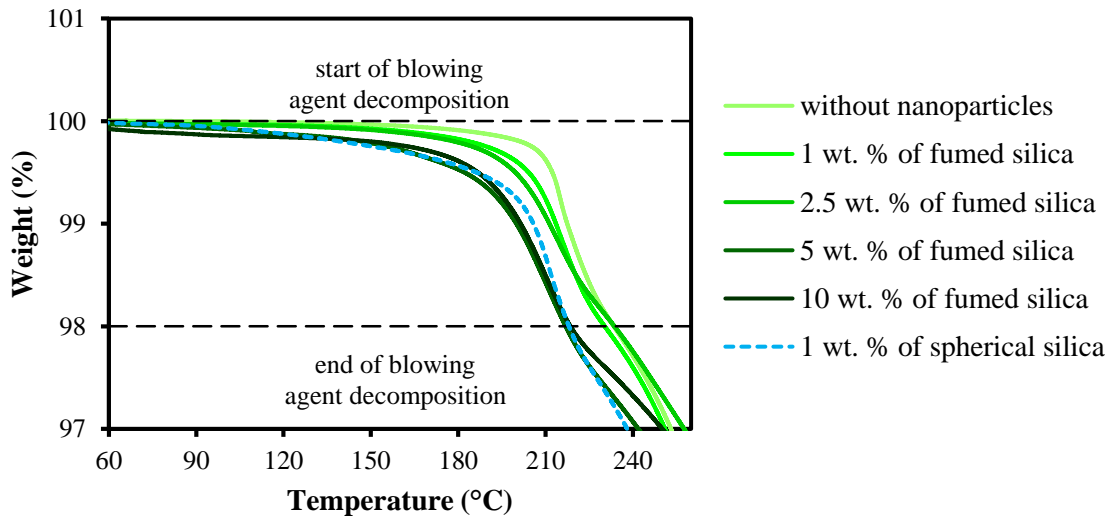
4.2.2 Effect of nanoparticles on the foaming process

Thermogravimetric analysis (TGA) was performed using filaments to investigate the effect of nanoparticles on the thermal behaviour of the thermal blowing agent and thus on the behaviour of the entire polymer system during processing.

Complete TGA curves:
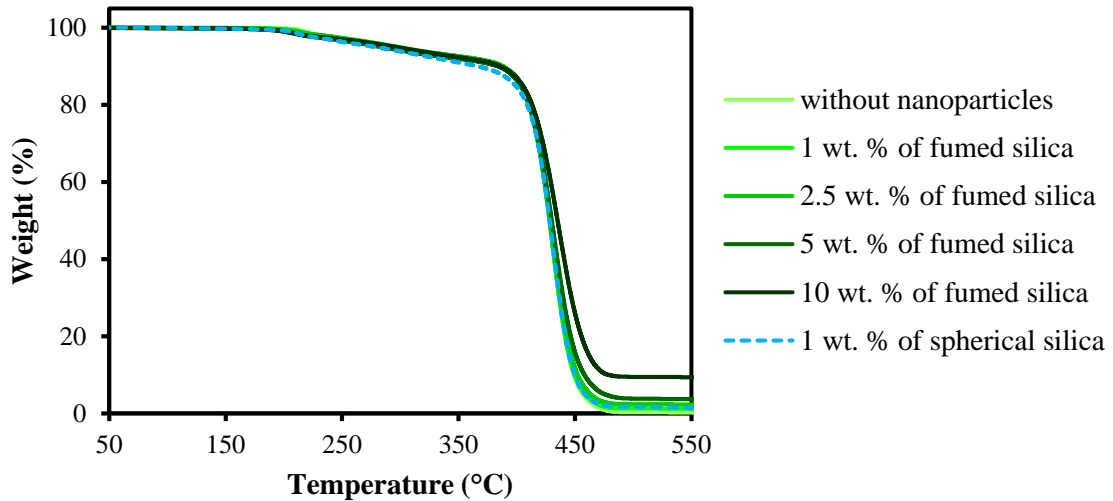
Detail of blowing agent decomposition area:

Figure 11: TGA curves of extruded filaments. **Top** – complete curves. **Bottom** – detail of area when the blowing agent was decomposed to gaseous products and causing foaming.

Figure 11 depicts the results of the TGA measurements. The TGA curves showed a similar shape for all the systems investigated differing more significantly only above approximately 450 °C. Here, the curves deviated from each other due to different amounts of nanosilica. However, magnifying the area in which the blowing agent decomposed, the significant effect of silica on this process was observed. Increasing silica content, the decomposition behaviour deviated more and more from the sample without nanoparticles. The sample with 1 wt. % of solvent-casted spherical silica deviated more than the sample with 1 wt. % of melt-blended fumed silica. To numerically compare this trend, the decomposition temperature of the blowing

agent was determined (Figure 12) – the peak value from the first derivation of the TGA curves. The blowing agent was the first component that decomposed in the system, so it was determined from the first peak value in the temperature range of 180–240 °C. Since it was a peak of derivation, it was more precisely the temperature at which the decomposition of the blowing agent had the fastest rate.
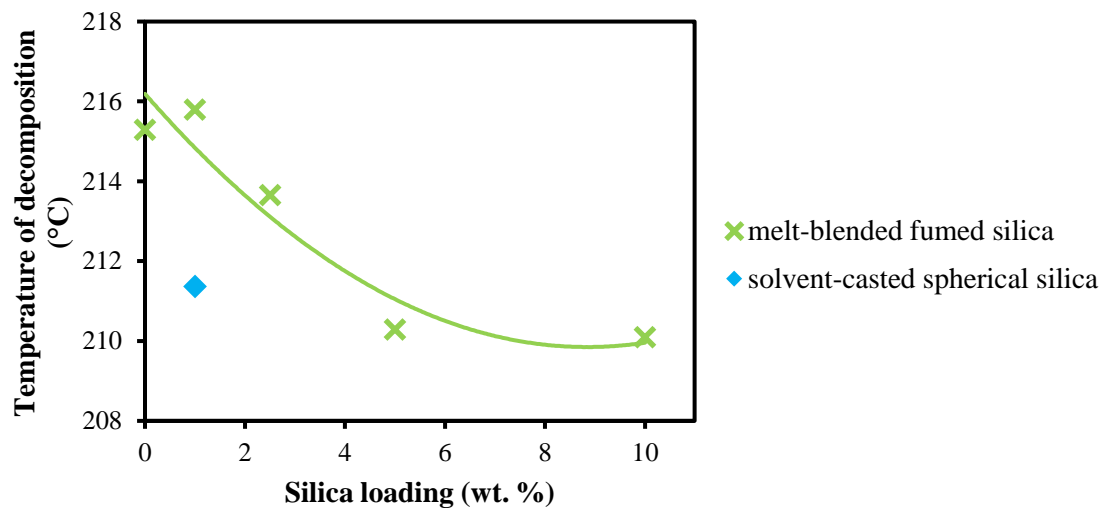
**Figure 12:** Dependence of blowing agent decomposition temperature on nanosilica loading.

Results in Figure 12 confirmed, that the decomposition temperature of the blowing agent decreased with an increasing amount of nanoparticles. During processing, decomposition of blowing agent in nanocomposites occurred at lower temperatures and the system was able to foam in a shorter time under the same temperature conditions. For spherical silica, this effect proved to be much more enhanced than for fumed silica. This was observed in practical terms in later experiments (paragraph 4.2.4) when 3D printed cylinders were foamed in a glass-aluminum mold at elevated temperatures. The system without nanoparticles needed 30 minutes to fill the mold. The sample with melt-blended fumed silica reduced this foaming time to 10 minutes and the sample with solvent-casted spherical silica to 5 minutes. Since the solvent-casted spherical nanosilica was distributed in the polymer matrix in the form of individual particles and its distribution homogeneity was on the nanoscale, it had a more significant effect on the surface energy of the blowing agent than large isolated aggregates of melt-blended fumed silica.

We ascribe this effect to the lowering the surface energy azodicarbonamide grains by silica nanoparticles making it easier to release gaseous products. A similar effect was observed by Zakiyan et. al [50] on the PS system but with a physical blowing agent (CO_2) because the nanoparticles reduced Gibb's free nucleation energy. Saha et al. [51] observed three different types of nanoparticles in PU foams and, conversely, observed an increase in thermal stability with the addition of nanoparticles. However, this could be due to the influence of nanoparticles on the synthesis of the PU polymer itself, when in their presence the polymer could crosslink more and thus cause an increase in thermal stability.

4.2.3 Effect of silica content on the foam porosity

The presence of nanoparticles had a major influence on the porosity, pore size, and spatial pore distribution of the resulting foam. In Figure 13, foamed HIPS with 2 wt. % of the foaming agent after single-screw extrusion is depicted. Samples had different nanosilica content – the first sample was without nanoparticles and then with 0.25, 1, 2.5, 5, and 10 wt. % of melt-blended fumed silica. All samples were prepared under the same conditions (temperature, rpm) to ensure the same foaming conditions and reproducibility. All samples showed a relatively uniform distribution of closed cells.
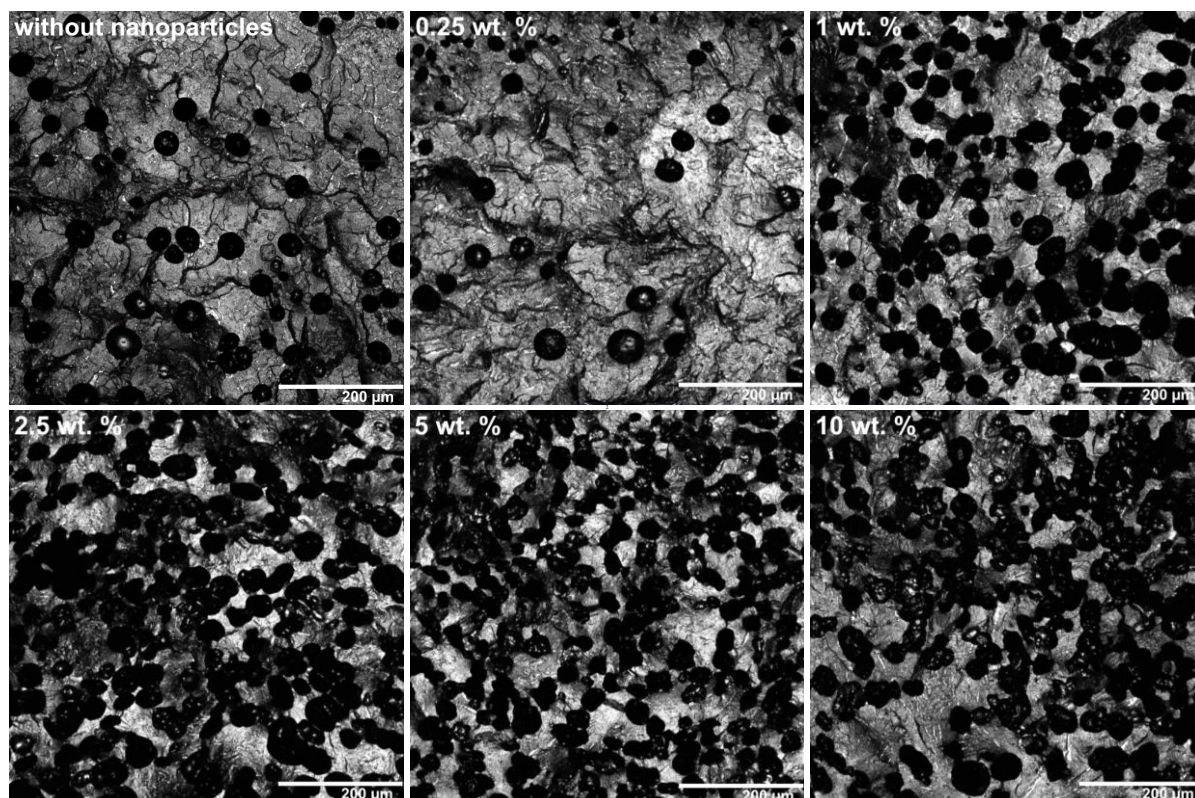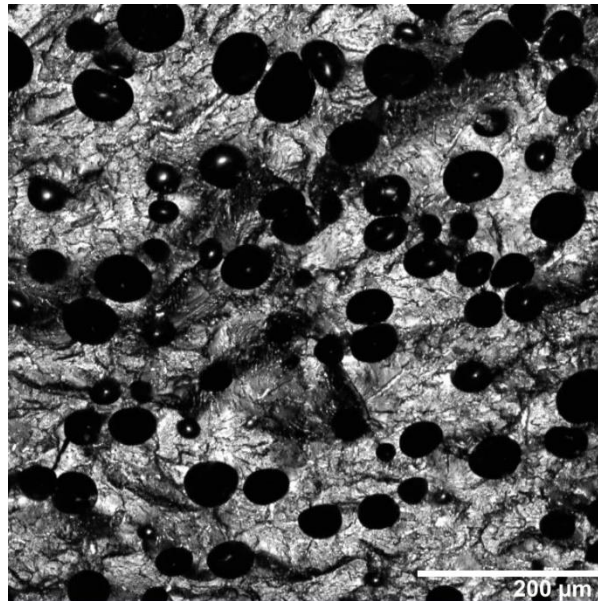

Figure 13: CLSM images of extruded filaments – HIPS with 2 wt. % of blowing agent after single-screw extrusion with different amounts of melt-blended fumed silica (without nanoparticles, with 0.25, 1, 2.5, 5, and 10 wt. % of fumed nanosilica).

It was clearly observable, that with higher silica content, the porosity of foams increased. It was shown that nanoparticles served as nucleating agents when a thermal chemical blowing agent was used. Bubble growth was facilitated on the surface of nanoparticles, creating more stable nucleation centers leading to a structure with a larger number of smaller pores.

Samples without nanoparticles and with 0.25 wt. % of fumed silica had discrete individual pores. In the sample with 1 wt. %, the number of pores highly raised and they slightly started to connect, but most of the pores were still separated. From the 2.5 to 10 wt. % of nanoparticles, the foam structure did not change significantly – all three samples showed the structure of a larger amount of mostly coalesced pores. All samples passed through the extruder at the same time, so they had also the same time for pore formation. Thus, the individual pores are all approximately the same size. Large pores were observed due to the connection of several of these individual pores, which grew close together. In the case of 10 wt. % of nanosilica, the ratio of connected bubbles seemed to be so high, that the start of open porosity could be

almost considered, but these large connected bubbles were not connected from a macroscopical point of view.

One sample with solvent-casted spherical silica was also extruded (Figure 14). The whole concentration series was not made due to the large demands on solvent material consumption, which represent an increased burden in financial and environmental points and due to more difficult way of solvent-casted samples preparation also time burden. Solvent-casted spherical silica sample showed the structure of a large number of individual pores and unlike 1 wt. % of fumed silica showed no coalescence of pores.


Figure 14: CLSM image of extruded filament – HIPS with 2 wt. % of blowing agent after single-screw extrusion with 1 wt. % of solvent-casted spherical nanosilica.

4.2.4 Structure of the 3D printed foams

When HIPS with the blowing agent was 3D printed below the decomposition temperature of azodicarbonamide, a very precise 3D printed structure was reached. No macroscopically observable porosity was produced. This property is an important premise e.g. for multi-material 3D printing, where the printing of the next material follows directly on the previous material to produce for example sandwich or gradient structures, where the foamable filament could be effectively used.

The microscopical structure of cylinders printed below the decomposition temperature of the blowing agent is depicted in Figure 15 (upper line). In the case of the sample without nanoparticles, it was possible to print a solid body without pores. When nanoparticles were added, the bubble formation occurred even below the standard decomposition temperature of azodicarbonamide. As was explained in paragraph 4.2.1, the presence of nanoparticles lowered the decomposition temperature of the blowing agent probably due to lowering surface energy around blowing agent grains, and thus gaseous decomposition products were released easier. Thus, it was possible to achieve porous structure even when 3D printing occurred at low-temperature conditions. During 3D printing, there was no shear stress as in the extruder, so the local overheating caused by shear friction could not be considered.
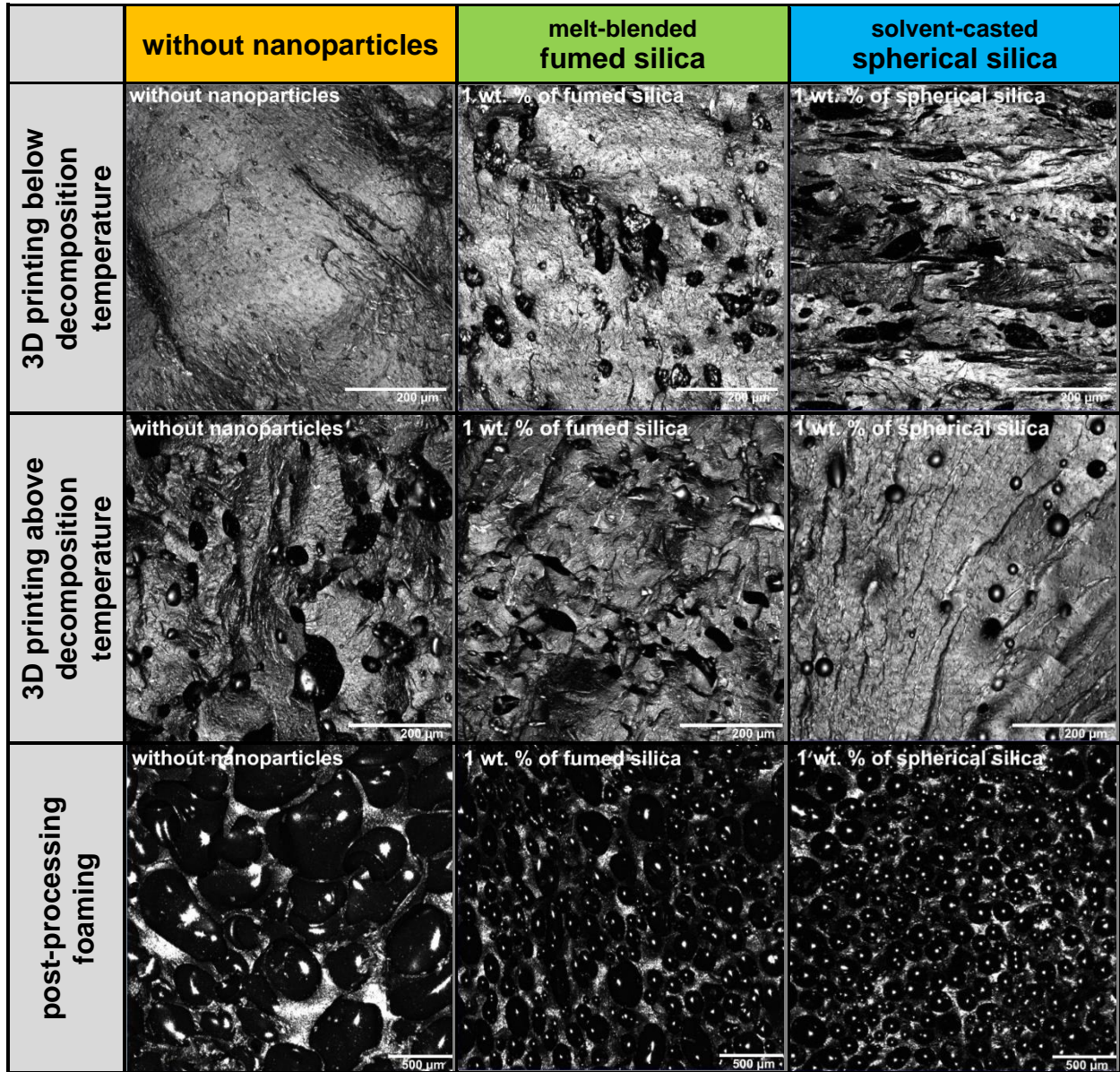
Figure 15: CLSM images of 3D printed cylinders based on HIPS and azodicarbonamide without nanoparticles (left column), with 1 wt. % of melt-blended fumed silica (middle column), and with 1 wt. % of solvent-casted spherical silica (right column). **Upper line** – after 3D printing below the decomposition temperature of the blowing agent (180 °C, scale bar 200 μm). **Middle line** – after 3D printing above the decomposition temperature of the blowing agent (220 °C, scale bar 200 μm). **Bottom line** – after post-processing in the pre-heated oven (200 °C, scale bar 500 μm).

When HIPS with the blowing agent was 3D printed above the decomposition temperature of azodicarbonamide with 100 % flow of the material through the printer, the expanding material took up more space than the compact unfoamed solid material and therefore overflows on the printed body arose. This inconvenience was suppressed by reducing the flow of material into the printer. The degree of this reduction was set experimentally so that the printed bodies had a shape precisely defined by the design, i.e. with no overflows or unprinted areas. The flow reduction was about 80 % in all three cases. The microscopical structure of cylinders printed above the decomposition temperature of the blowing agent is depicted in Figure 15 (middle line). The homogenous microporosity was formed in all three cases (without nanoparticles,

with melt-blended fumed silica, and with solvent-casted spherical silica). Printing above the decomposition temperature of azodicarbonamide allowed producing of directly foamed bodies with a precise outer structure designed by software without any post-processing treatment. Needless to say, that the resulting pores were slightly compressed by the printer nozzle during the deposition of the newly printed layer, i.e. they were reduced in size.

Cylinders, which were 3D printed below the decomposition temperature of the blowing agent, were then thermally treated in a pre-heated oven – they were subjected to post-processing foaming. 3D printed cylinders were closed in the aluminum mold with glass bases with a diameter of 120 % compared to the diameter of the original cylinders and foamed in the oven at 200 °C. Foaming time was set experimentally so that the cylinder was perfectly foamed, i.e. it just took its place in the mold without overflows or unfilled spots. Foaming time varied significantly depending on the material. Without nanoparticles, the foaming time was 30 minutes. With fumed silica distributed in the material in the form of micro aggregates, the foaming time was 10 minutes, i.e. it was reduced by 66.7 %. In the case of spherical silica distributed in the material in the form of individual nanoparticles, the foaming time was 5 minutes, i.e. reduced by 83.3 %. Another fact that contributed to the more rapid foaming was that the samples with nanoparticles had small pores already immediately after 3D printing, unlike the sample without nanoparticles. These pores then served as precursors for post-process foaming and facilitated the formation of larger pores. Post-processing foaming after 3D printing allowed the production of material with even larger pores, i.e. with even lower density. It allowed to print small objects and then foam them into larger ones with little material consumption. The microscopical structure of cylinders after post-processing foaming is depicted in Figure 15 (bottom line). The effect of nanoparticles was striking in this case. Large pores were formed in the sample without nanoparticles. The size of the pores was significantly decreased and the number of pores was increased when nanoparticles were added. Nanoparticles served as heterogeneous nucleation centers during bubble growth and thus support growing large amounts of smaller pores. In the case of solvent-casted spherical silica, pores seemed to be smaller and more homogenous than in the case of melt-blended fumed silica.

4.2.5 Tensile properties of filaments

Stress-strain curves of the materials investigated are shown in Figure 16. Tensile behaviour with high deformations was observable in the pure HIPS sample, sample without nanoparticles or only with a small nanoparticle loading (0.25 wt. % of fumed silica). A further increase of nanoparticle content led to embrittlement and a decrease in the stress plateau region and elongation. Pure HIPS, sample without nanoparticles, and sample with 0.25 wt. % of fumed silica had significant overshoot in yield point area with strain softening region. On the other hand, this overshoot disappeared and the yield point was followed only by gradual strain hardening in samples with higher nanoparticle content. The sample with 10 wt. % of fumed silica showed such a brittle behaviour, that not all of the test specimens reached the yield point and their failure occurred immediately after the linear region of elastic deformation.
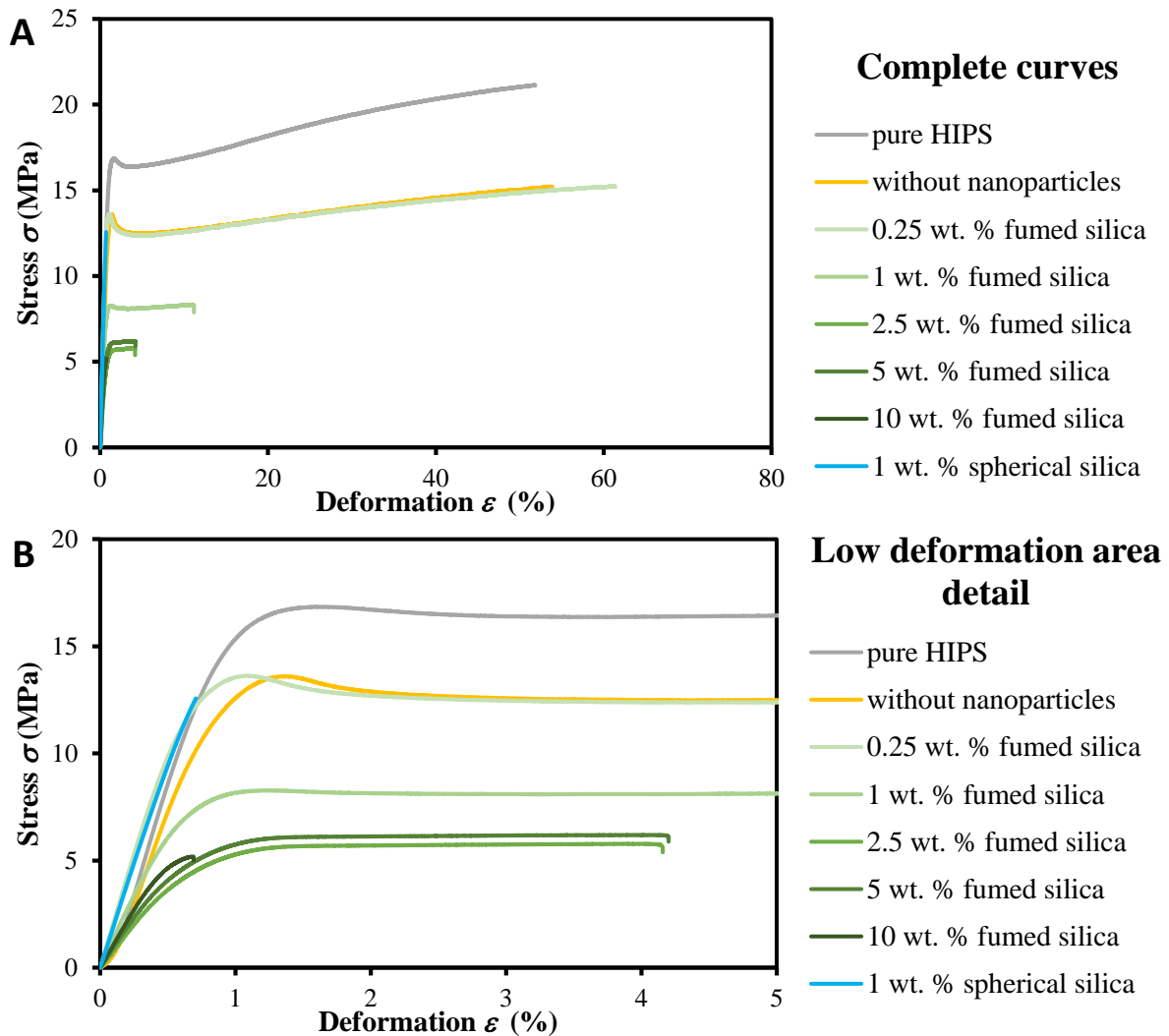
Figure 16: Representative tensile stress-strain curves of extruded filaments. **Top** – complete curves. **Bottom** – detail of low deformation area. All curves of specimens are in the appendix.

Very significant differences in the mechanical response were observed between samples with 1 wt. % of the different silica. Sample with 1 wt. % of melt-blended fumed silica showed still ductile behaviour, although it reached maximally half deformations than pure HIPS. In contrast, the sample with 1 wt. % of solvent-casted spherical silica was the most brittle of all the filaments but was able to achieve higher stress than other silica samples.

The different behaviour of samples with 1 wt. % of silica (solvent-casted spherical silica or melt-blended fumed silica) was due to how nanoparticles were incorporated into the polymer matrix. While fumed nanosilica particles remained exclusively in the PS matrix, spherical nanosilica was also incorporated at the interface of the PS-rubber particles and in the occluded rubber particles themselves (Figure 8). Disruption of the PS-rubber phase interface and reinforcement of the rubber particles themselves leaded to a loss of the toughening rubber effect. During deformation, there was no effective interface extraction of rubber fibrils, on which energy dissipation would occur. The sample with spherical silica thus shifted its mechanical properties towards the properties of pure PS away from the properties of rubber – it lost ductility but was able to withstand higher stresses.

Only a small amount of nanoparticles was sufficient enough to effectively modify the mechanical properties. A higher content worsened the mechanical properties in an undesirable way and made the cost of the material more expensive. Xu et al. [52] concluded during their research of PU foams with organoclay nanofiller, that compressive and tensile strength was maximized at 2 phr ($\approx 1.96\%$) of the nanofiller. Up to this value, the nanoclay filler increased the strength, at higher contents the strength decreased. They also observed that the average pore size decreased to 2 phr and increased when exceeded. Zhang et al. [53] observed very similar behaviour directly on the HIPS system with TiO_2 nanoparticles. They observed maximized notched impact strength, tensile strength, and tensile elastic modulus at 2 % of nanofiller. The conclusions of these independent researches are practically identical to the conclusions of this dissertation work. As for the practical observation of the filaments examined in this work, filaments with a higher silica content (2.5 wt. % and higher) were no longer suitable for 3D printing – filaments diameter fluctuated and the surface roughness of the filament increased.

4.2.6 Compressive behaviour of 3D printed foams

Compressive stress-strain curves of the cylinders are in Figure 17, while the top graph shows the deformation response of cylinders printed below the decomposition temperature of the blowing agent, the middle graph shows the deformation response of cylinders printed above the decomposition temperature and the bottom graph shows cylinders after post-processing foaming.
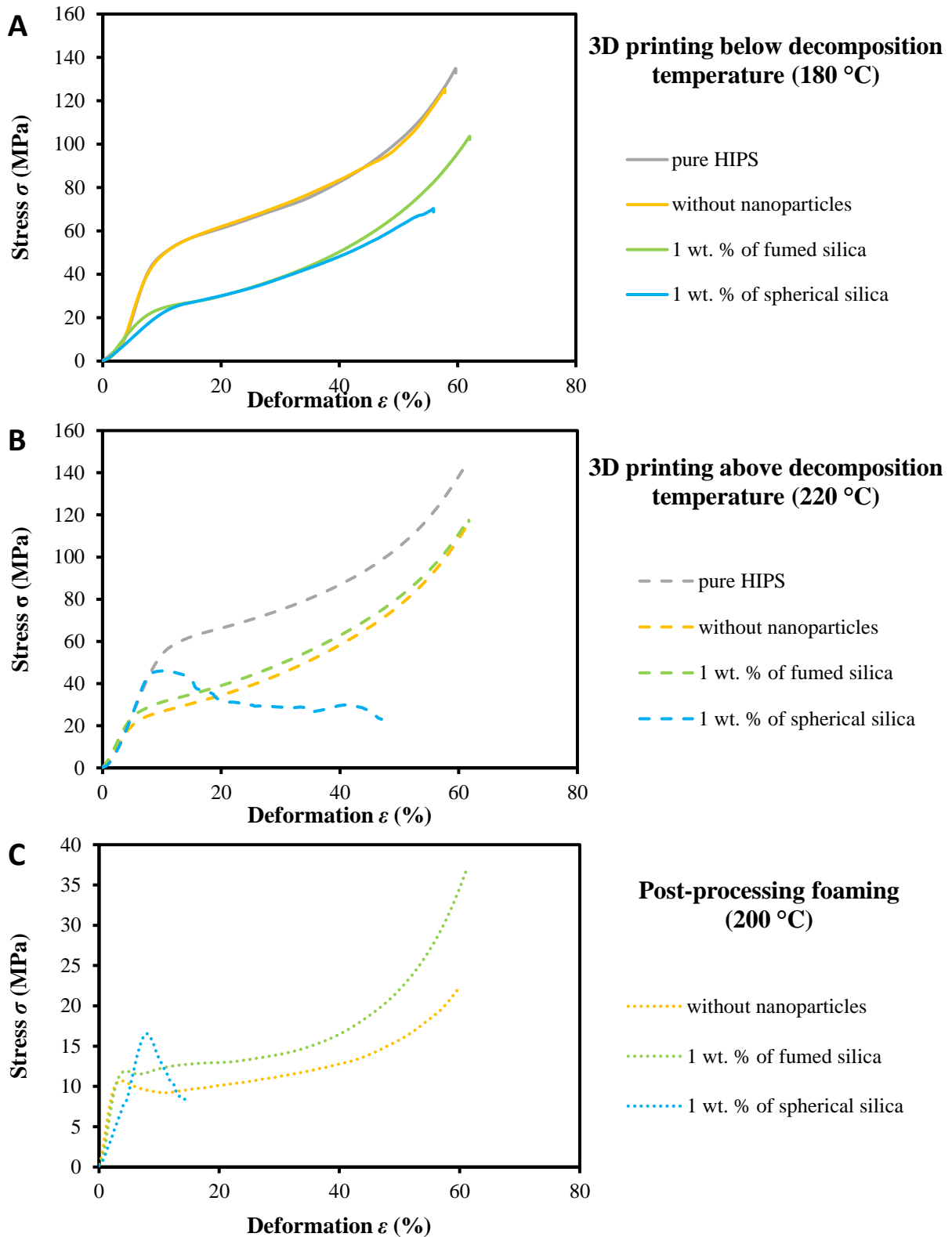
Figure 17: Representative compressive stress-strain curves of 3D printed cylinders. **Top** – Cylinders printed below the decomposition temperature of the blowing agent. **Middle** – Cylinders printed above the decomposition temperature of the blowing agent. **Bottom** – Cylinders after post-processing foaming. All curves of all specimens are in the appendix.

In the case of samples 3D printed below the decomposition temperature of the blowing agent, the results fully corresponded to the structure of the samples. Samples without pores (pure HIPS and HIPS without nanoparticles) could withstand higher compressive stresses. In contrast, samples with nanoparticles that contained microscopically observable porosity showed after linear elastic regime lower plastic collapse stress. For all samples printed below the decomposition temperature, continuous strain hardening occurred after the linear regime without overshoot at yield point and without constant plateau regime.

In the case of samples 3D printed above the decomposition temperature of the blowing agent, the highest stress was again withstood by pure HIPS without porosity. Porous samples without nanoparticles and with fumed silica showed lower plastic collapse stress after the elastic region with gradual strain hardening without overshoot on yield point. On the other hand, the sample with spherical silica reached higher stresses within the linear elastic region than other porous samples, its elastic region was followed by a significant overshoot on yield and some of its specimens switched to a constant plateau mode, some specimens collapsed before the plateau regimen.

Pure HIPS was not included among the samples after post-process foaming, because as the only sample it did not contain a blowing agent, it was not possible to foam it and the post-processing thermal treatment did not make sense for this sample. All other samples had approximately the same porosity and density, but the sample without nanoparticles had significantly larger pores and significantly lower cell density. This difference in structure was well reflected in the deformation response when due to the finer pore structure of the samples with nanoparticles, higher plastic collapse stress was achieved than in the case of samples without nanoparticles. All samples showed a significant overshoot in the yield region after the elastic region followed by a plateau regime. Only the sample with spherical silica failed before the plateau regimen, but this sample showed the highest yield point peak.

The effective improvement of mechanical properties by nanoparticles was demonstrated especially in samples where nanoparticles were allowed to fully manifest during porosity formation, i.e. post-processing foaming because the system was not limited by the short time or limited space for foaming. Unlike samples directly after 3D printing, when porosity formation was significantly affected by the deposition of individual printed layers and the forming pores were spread with an extruder nozzle. Samples with solvent-casted spherical silica were more brittle due to the disruption of the rubber effect by nanoparticles.

5 CONCLUSION

Cellular nanocomposites with structure organized on multiple hierarchical levels were prepared using the additive manufacturing technique. The principle governing the self-assembly of silica in glassy polymer nanocomposites prepared by solvent-casting was found. The difference in the Hildebrand solubility parameter between the polymer and the solvent was proved to be the decisive parameter. In the case of a small difference between the solubility parameters, the particles were coated with an adsorbed layer of compact polymer coils which stabilized good dispersion. If the difference between the parameters was large, the polymer chains adsorbed on one particle were more expanded and flexible and therefore did not form a steric barrier for another particle, and contact aggregation occurred. The expanded coil could act as bridging molecules within a cluster. Another important parameter was the ζ-potential of nanoparticles in a given solvent, which represented the charge on the silica surface and the ability of the solvent to create a solvation shell around the particles.

Three solvents producing very good dispersion of nanoparticles in glassy PS were also investigated in systems with two-component polymer blend HIPS. Cyclohexanone dissolved both components of the HIPS – PS matrix and rubber particles. Thus, small spherical nanosilica was capable to penetrate into occluded rubber particles and assembled in the PS-rubber interface. DMAC and DMF dissolved selectively PS and did not dissolve PBR particles. Therefore, silica was unable to enter the rubber particles and remained only in the PS matrix. Sufficiently small particles with spherical geometry and non-selective solvent were needed for the efficient incorporation of silica into the rubber particles of the HIPS.

HIPS nanocomposite with solvent-casted spherical silica (prepared in cyclohexanone) and melt-blended fumed nanosilica were used for the preparation of foamable filaments for 3D printing using azodicarbonamide as the blowing agent. Azodicarbonamide had a sufficiently high decomposition temperature to prevent its unwanted foaming during processing (filament extrusion, 3D printing), but at the same time, its decomposition temperature was low enough to avoid excessive HIPS degradation.

It has been shown that nanoparticles behaved as nucleating agents for the pores. Pore growth was facilitated on the surface of the nanoparticles, creating more stable nucleation centers leading to foams with a larger amount with smaller pores. The formed pores were always closed. Nanoparticles were the most effective at low concentrations below 1 wt. % to create foams with small pores.

The presented foamable HIPS-nanoparticle material for 3D printing offered a huge variability of possibilities – a non-foamed solid sample was printed, a porous sample was directly printed as well or the sample was foamed to large dimensions after printing by post-processing foaming in the oven. And all of this was done using one filament by a simple variation of printer settings.

Mechanical properties of the cellular foamable materials were also analyzed to characterize prepared systems. Despite the used additives forming a small microscopically observable porosity in the filaments themselves, the quality of the foamable filaments for 3D printing was comparable to the pure HIPS standardly used for 3D printing as was shown by tensile tests. In the case of compressive properties of 3D printed samples, the addition of nanoparticles in many cases even improved the properties of the material compared to pure HIPS.

The solvent-casted spherical silica system was more similar to the nanoparticle-free system (in terms of density, cell density, porosity and did not form observable porosity during extrusion, the filaments were smooth), which was advantageous for processing. At the same time, it had more modified properties than a fumed silica system after 3D printing. The only disadvantage of this system was the higher brittleness due to the suppression of the rubber effect in HIPS by the presence of nanoparticles at the PS-rubber interface and in the rubber particles. But despite this embrittlement, the 3D material was printable and showed, for example, an increase in the modulus of elasticity.

The material based on HIPS and azodicarbonamide with the possible addition of nanoparticles developed in this dissertation was essentially a finished and characterized product that could contribute to the satisfaction of the growing demand for 3D printing materials with enhanced specialized properties.

6 BIBLIOGRAPHY

[1] WEGST, Ulrike, Hao BAI, Eduardo SAIZ, Antoni TOMSIA a Robert RITCHIE. Bioinspired structural materials. *Nature Materials*. 2015, **14**(1), 23-36. ISSN 1476-1122. Available at: doi:10.1038/nmat4089

[2] GIBSON, Lorna. Biomechanics of cellular solids. *Journal of Biomechanics*. 2005, **38**(3), 377-399. ISSN 00219290. Available at: doi:10.1016/j.jbiomech.2004.09.027

[3] FRATZL, Peter a Richard WEINKAMER. Nature's hierarchical materials. *Progress in Materials Science*. 2007, **52**(8), 1263-1334. ISSN 00796425. Available at: doi:10.1016/j.pmatsci.2007.06.001

[4] DIXON, P. a L. GIBSON. The structure and mechanics of Moso bamboo material. *Journal of The Royal Society Interface*. 2014, **11**(99), 20140321-20140321. ISSN 1742-5689. Available at: doi:10.1098/rsif.2014.0321

[5] WOESZ, Alexander, James WEAVER, Murat KAZANCI, Yannicke DAUPHIN, Joanna AIZENBERG, Daniel MORSE a Peter FRATZL. Micromechanical properties of biological silica in skeletons of deep-sea sponges. *Journal of Materials Research*. 2006, **21**(08), 2068-2078. ISSN 0884-2914. Available at: doi:10.1557/jmr.2006.0251

[6] KAO, Joseph, Kari THORKELSSON, Peter BAI, Benjamin RANCATORE a Ting XU. Toward functional nanocomposites: taking the best of nanoparticles, polymers, and small molecules. *Chem. Soc. Rev*. 2013, **42**(7), 2654-2678. ISSN 0306-0012. Available at: doi:10.1039/C2CS35375J

[7] FENG, Jiawei, Jianzhong FU, Ce SHANG, Zhiwei LIN, Xiaomiao NIU a Bin LI. Efficient generation strategy for hierarchical porous scaffolds with freeform external geometries. *Additive Manufacturing*. 2020, **31**. ISSN 22148604. Available at: doi:10.1016/j.addma.2019.100943

[8] YANG, Xiao-Yu, Li-Hua CHEN, Yu LI, Joanna ROOKE, Clément SANCHEZ a Bao-Lian SU. Hierarchically porous materials: synthesis strategies and structure design. *Chemical Society Reviews*. 2017, **46**(2), 481-558. ISSN 0306-0012. Available at: doi:10.1039/C6CS00829A

[9] ZENG, C., X. HAN, L.J. LEE, K.W. KOELLING a D.L. TOMASKO. Polymer–Clay Nanocomposite Foams Prepared Using Carbon Dioxide. *Advanced Materials*. 2003, **15**(20), 1743–1747. ISSN 0935-9648. Available at: doi:10.1002/adma.200305065

[10] LEE, L, C ZENG, X CAO, X HAN, J SHEN a G XU. Polymer nanocomposite foams. *Composites Science and Technology*. 2005, **65**(15-16), 2344-2363. ISSN 02663538. Available at: doi:10.1016/j.compscitech.2005.06.016

[11] JANCAR, J., J.F. DOUGLAS, F.W. STARR, S.K. KUMAR, P. CASSAGNAU, A.J. LESSER, S.S. STERNSTEIN a M.J. BUEHLER. Current issues in research on structure–property relationships in polymer nanocomposites. *Polymer*. 2010, **51**(15), 3321-3343. ISSN 00323861. Available at: doi:10.1016/j.polymer.2010.04.074

[12] AKSIT, Merve, Chunjing ZHAO, Bastian KLOSE, Klaus KREGER, Hans-Werner SCHMIDT a Volker ALTSTÄDT. Extruded Polystyrene Foams with Enhanced Insulation and Mechanical Properties by a Benzene-Trisamide-Based Additive. *Polymers*. 2019, **11**(2), 1–10. ISSN 2073-4360. Available at: doi:10.3390/polym11020268

[13] LOBOS, Juan a Sachin VELANKAR. How much do nanoparticle fillers improve the modulus and strength of polymer foams?. *Journal of Cellular Plastics*. 2016, **52**(1), 57-88. ISSN 0021-955X. Available at: doi:10.1177/0021955X14546015

[14] WICKLEIN, Bernd, Andraž KOCJAN, German SALAZAR-ALVAREZ, Federico CAROSIO a Giovanni CAMINO. Thermally insulating and fire-retardant lightweight anisotropic foams based on nanocellulose and graphene oxide. *Nature Nanotechnology*. 2015, **10**(3), 277–283. ISSN 1748-3387. Available at: doi:10.1038/NNANO.2014.248

[15] JIANG, Yanhui a Qiming WANG. Highly-stretchable 3D-architected Mechanical Metamaterials. *Scientific Reports*. 2016, **6**(1). ISSN 2045-2322. Available at: doi:10.1038/srep34147

[16] LUONG, Dung. Structure and Compressive Properties of Invar-Cenosphere Syntactic Foams. *Materials*. 2016, **9**(2), 1–16. ISSN 1996-1944. Available at: doi:10.3390/ma9020115

[17] SALLEH, Zulzamri, Md MAINUL ISLAM, Jayantha ANANDA EPAARACHCHI a Haibin SU. Mechanical properties of sandwich composite made of syntactic foam core and GFRP skins. *AIMS Materials Science*. 2016, **3**(4), 1704-1727. ISSN 2372-0484. Available at: doi:10.3934/matersci.2016.4.1704

[18] GUPTA, Nikhil, Dinesh PINISETTY a Vasanth SHUNMUGASAMY. *Reinforced polymer matrix syntactic foams*. 1. New York: Springer, 2013. ISBN 978-3-319-01242-1.

[19] PRAKASH, A., William SWAM a Alec STRACHAN. The thermal decomposition of azodicarbonamide (1,1′-azobisformamide). *J. Chem. Soc., Perkin Trans. 2*. 1975, (1), 46-50. ISSN 0300-9580. Available at: doi:10.1039/P29750000046

[20] ZARYBNICKA, Klara, Frantisek ONDREAS, Petr LEPCIO, Michal KALINA, Marek ZBONCAK a Josef JANCAR. Thermodynamic Parameters Controlling Nanoparticle Spatial Packing in Polymer Solutions. *Macromolecules*. 2020, **53**(19), 8704-8713. ISSN 0024-9297. Available at: doi:10.1021/acs.macromol.0c00698

[21] JOUAULT, Nicolas, Dan ZHAO a Sanat KUMAR. Role of Casting Solvent on Nanoparticle Dispersion in Polymer Nanocomposites. *Macromolecules*. 2014, **47**(15), 5246-5255. ISSN 0024-9297. Available at: doi:10.1021/ma500619g

[22] LEPCIO, Petr. *Effect of sub-mictometer sctructural features on rheology of polymer nanocomposites*. Brno, 2018. Doctoral thesis. Brno University of Technology.

[23] HANSEN, Charles M. *Hansen solubility parameters: a user's handbook*. 2nd ed. Boca Raton: CRC Press, 2007. ISBN 978-084-9372-483.

[24] VAN DER BEEK, G., M. STUART, G. FLEER a J. HOFMAN. Segmental adsorption energies for polymers on silica and alumina. *Macromolecules*. 1991, **24**(25), 6600-6611. ISSN 0024-9297. Available at: doi:10.1021/ma00025a009

[25] LEPCIO, Petr, Frantisek ONDREAS, Klara ZARYBNICKA, Marek ZBONCAK, Ondrej CAHA a Josef JANCAR. Bulk polymer nanocomposites with preparation protocol governed nanostructure: the origin and properties of aggregates and polymer bound clusters. *Soft Matter*. 2018, **14**(11), 2094-2103. ISSN 1744-683X. Available at: doi:10.1039/C8SM00150B

[26] KUMAR, Ajeet a Chandra DIXIT. Methods for characterization of nanoparticles. *Advances in Nanomedicine for the Delivery of Therapeutic Nucleic Acids*. Elsevier, 2017, , 43-58. ISBN 9780081005576. Available at: doi:10.1016/B978-0-08-100557-6.00003-1

[27] ZÁRYBNICKÁ, Klára, František ONDREÁŠ, Petr LEPCIO, Chao CHEN a Josef JANČÁŘ. In-situ self-assembly of silica nanoparticles into microfibers with potential to reinforce polymers. *Nanocon: Proceedings 11th International Conference on Nanomaterials - Research & Application*. 2020, , 673-678. Available at: doi:10.37904/nanocon.2019.8489

[28] HASHEMI, Amir, Nicolas JOUAULT, Gregory WILLIAMS, Dan ZHAO, Kevin CHENG, Jeffrey KYSAR, Zhibin GUAN a Sanat KUMAR. Enhanced Glassy State Mechanical Properties of Polymer Nanocomposites via Supramolecular Interactions. *Nano Letters*. 2015, **15**(8), 5465-5471. ISSN 1530-6984. Available at: doi:10.1021/acs.nanolett.5b01859

[29] SVOBODA, Roman. How to determine activation energy of glass transition. *Journal of Thermal Analysis and Calorimetry*. 2014, **118**(3), 1721-1732. ISSN 1388-6150. Available at: doi:10.1007/s10973-014-4077-8

[30] ONDREAS, Frantisek, Petr LEPCIO, Marek ZBONCAK, Klara ZARYBNICKA, Leon GOVAERT a Josef JANCAR. Effect of Nanoparticle Organization on Molecular Mobility and Mechanical Properties of Polymer Nanocomposites. *Macromolecules*. 2019, **52**(16), 6250-6259. ISSN 0024-9297. Available at: doi:10.1021/acs.macromol.9b01197

[31] KALFUS, J. a J. JANCAR. Immobilization of polyvinylacetate macromolecules on hydroxyapatite nanoparticles. *Polymer*. 2007, **48**(14), 3935-3937. ISSN 00323861. Available at: doi:10.1016/j.polymer.2007.04.049

[32] BERRIOT, Julien, Hélène MONTES, François LEQUEUX, Didier LONG a Paul SOTTA. Evidence for the Shift of the Glass Transition near the Particles in Silica-Filled Elastomers. *Macromolecules*. 2002, **35**(26), 9756-9762. ISSN 0024-9297. Available at: doi:10.1021/ma0212700

[33] BERRIOT, J., H. MONTES, F. LEQUEUX, D. LONG a P. SOTTA. Gradient of glass transition temperature in filled elastomers. *Europhysics Letters (EPL)*. 2003, **64**(1), 50-56. ISSN 0295-5075. Available at: doi:10.1209/epl/i2003-00124-7

[34] EMAMY, Hamed, Sanat KUMAR a Francis STARR. Diminishing Interfacial Effects with Decreasing Nanoparticle Size in Polymer-Nanoparticle Composites. *Physical Review Letters*. 2018, **121**(20). ISSN 0031-9007. Available at: doi:10.1103/PhysRevLett.121.207801

[35] ZBONCAK, Marek, Frantisek ONDREAS, Vojtech UHLIR, Petr LEPCIO, Jan MICHALICKA a Josef JANCAR. *Translation of segment scale stiffening into macroscale reinforcement in polymer nanocomposites*. 2019. ISSN 0032-3888. Available at: doi:10.1002/pen.25317

[36] TANNENBAUM, Rina, Melissa ZUBRIS, Kasi DAVID, Dan CIPRARI, Karl JACOB, Iwona JASIUK a Nily DAN. FTIR Characterization of the Reactive Interface of Cobalt Oxide Nanoparticles Embedded in

Polymeric Matrices. *The Journal of Physical Chemistry B*. 2006, **110**(5), 2227-2232. ISSN 1520-6106. Available at: doi:10.1021/jp054469y

[37] CIPRARI, Dan, Karl JACOB a Rina TANNENBAUM. Characterization of Polymer Nanocomposite Interphase and Its Impact on Mechanical Properties. *Macromolecules*. 2006, **39**(19), 6565-6573. ISSN 0024-9297. Available at: doi:10.1021/ma0602270

[38] CHENG, Shiwang, Bobby CARROLL, Wei LU et al. Interfacial Properties of Polymer Nanocomposites: Role of Chain Rigidity and Dynamic Heterogeneity Length Scale. *Macromolecules*. 2017, **50**(6), 2397-2406. ISSN 0024-9297. Available at: doi:10.1021/acs.macromol.6b02816

[39] JOUAULT, Nicolas, Florent DALMAS, François BOUÉ a Jacques JESTIN. Multiscale characterization of filler dispersion and origins of mechanical reinforcement in model nanocomposites. *Polymer*. 2012, **53**(3), 761-775. ISSN 00323861. Available at: doi:10.1016/j.polymer.2011.12.001

[40] GENIX, Anne-Caroline, Vera BOCHAROVA, Bobby CARROLL et al. Understanding the Static Interfacial Polymer Layer by Exploring the Dispersion States of Nanocomposites. *Applied Materials and Interfaces*. 2019, **11**(19), 17863-17872. ISSN 1944-8244. Available at: doi:10.1021/acsami.9b04553

[41] KIM, So a Charles ZUKOSKI. Role of Polymer Segment–Particle Surface Interactions in Controlling Nanoparticle Dispersions in Concentrated Polymer Solutions. *Langmuir*. 2011, **27**(17), 10455-10463. ISSN 0743-7463. Available at: doi:10.1021/la201704u

[42] STERNSTEIN, S. a Ai-Jun ZHU. Reinforcement Mechanism of Nanofilled Polymer Melts As Elucidated by Nonlinear Viscoelastic Behavior. *Macromolecules*. 2002, **35**(19), 7262-7273. ISSN 0024-9297. Available at: doi:10.1021/ma020482u

[43] HARTON, Shane, Sanat KUMAR, Hoichang YANG et al. Immobilized Polymer Layers on Spherical Nanoparticles. *Macromolecules*. 2010, **43**(7), 3415-3421. ISSN 0024-9297. Available at: doi:10.1021/ma902484d

[44] JOUAULT, Nicolas, Joseph MOLL, Dong MENG, Kendra WINDSOR, Stacy RAMCHARAN, Clare KEARNEY a Sanat KUMAR. Bound Polymer Layer in Nanocomposites. *ACS Macro Letters*. 2013, **2**(5), 371-374. ISSN 2161-1653. Available at: doi:10.1021/mz300646a

[45] KALFUS, J. a J. JANCAR. Relaxation processes in PVAc-HA nanocomposites. *Journal of Polymer Science Part B: Polymer Physics*. 2007, **45**(11), 1380-1388. ISSN 08876266. Available at: doi:10.1002/polb.21139

[46] KUMAR, Sanat, Nicolas JOUAULT, Brian BENICEWICZ a Tony NEELY. Nanocomposites with Polymer Grafted Nanoparticles. *Macromolecules*. 2013, **46**(9), 3199-3214. ISSN 0024-9297. Available at: doi:10.1021/ma4001385

[47] ANDERSON, Benjamin a Charles ZUKOSKI. Rheology and Microstructure of an Unentangled Polymer Nanocomposite Melt. *Macromolecules*. 2008, **41**(23), 9326-9334. ISSN 0024-9297. Available at: doi:10.1021/ma801415e

[48] F. BEHBAHANI, Alireza, S. VAEZ ALLAEI, Ghodratollah H. MOTLAGH, Hossein ESLAMI a Vagelis HARMANDARIS. Structure and dynamics of stereo-regular poly(methyl-methacrylate) melts through atomistic molecular dynamics simulations. *Soft Matter*. 2018, **14**(8), 1449-1464. ISSN 1744-683X. Available at: doi:10.1039/C7SM02008B

[49] ONDREAS, Frantisek a Josef JANCAR. Temperature, Frequency, and Small Static Stress Dependence of the Molecular Mobility in Deformed Amorphous Polymers near Their Glass Transition. *Macromolecules*. 2015, **48**(13), 4702-4716. ISSN 0024-9297. Available at: doi:10.1021/acs.macromol.5b00550

[50] ZAKIYAN, Seyed, Mohamad FAMILI a Mohammad AKO. Controlling foam morphology of polystyrene via surface chemistry, size and concentration of nanosilica particles. *Journal of Materials Science*. 2014, **49**(18), 6225-6239. ISSN 0022-2461. Available at: doi:10.1007/s10853-014-8347-4

[51] SAHA, M.C., Md.E. KABIR a S. JEELANI. Enhancement in thermal and mechanical properties of polyurethane foam infused with nanoparticles. *Materials Science and Engineering: A*. 2008, **479**(1-2), 213-222. ISSN 09215093. Available at: doi:10.1016/j.msea.2007.06.060

[52] XU, Zhongbin, Xiling TANG, Aijuan GU a Zhengping FANG. Novel preparation and mechanical properties of rigid polyurethane foam/organoclay nanocomposites. *Journal of Applied Polymer Science*. 2007, **106**(1), 439-447. ISSN 00218995. Available at: doi:10.1002/app.26497

[53] ZHANG, Jinzhu, Xin WANG, Lude LU, Dan LI a Xujie YANG. Preparation and performance of high-impact polystyrene (HIPS)/nano-TiO2 nanocomposites. *Journal of Applied Polymer Science*. 2003, **87**(3), 381-385. ISSN 0021-8995. Available at: doi:10.1002/app.11302